

## Guide to Reference and Standard Ionosphere Models

AIAA standards are copyrighted by the American Institute of Aeronautics and Astronautics (AIAA), 1801 Alexander Bell Drive, Reston, VA 20191-4344 USA. All rights reserved.

AIAA grants you a license as follows: The right to download an electronic file of this AIAA standard for temporary storage on one computer for purposes of viewing, and/or printing one copy of the AIAA standard for individual use. Neither the electronic file nor the hard copy print may be reproduced in any way. In addition, the electronic file may not be distributed elsewhere over computer networks or otherwise. The hard copy print may only be distributed to other employees for their internal use within your organization.



**ANSI/AIAA  
G-034-1998**

**American National Standard**

# **Guide to Reference and Standard Ionosphere Models**

Sponsor

**American Institute of Aeronautics and Astronautics**

Approved July 15, 1999

**American National Standards Institute**

## **Abstract**

This standard provides guidelines for selecting ionospheric models for engineering design or scientific research. The Guide describes the content of the models, uncertainties and limitations, technical basis, databases from which the models are formed, publication references, and sources of computer codes for approximately 30 ionospheric models. The models cover the altitude range from the Earth's surface to approximately 10,000 kilometers. This Guide is intended to assist communication ( $C^3I$ ) and space system designers and developers, geophysicists, space physicists, and climatologists in understanding available models and comparing sources of data and interpreting engineering and scientific results based on different ionospheric models.

## American National Standard

Approval of an American National Standard requires verification by ANSI that the requirements for due process, consensus, and other criteria have been met by the standards developer.

Consensus is established when, in the judgment of the ANSI Board of Standards Review, substantial agreement has been reached by directly and materially affected interests. Substantial agreement means much more than a simple majority, but not necessarily unanimity. Consensus requires that all views and objections be considered, and that a concerted effort be made toward their resolution.

The use of American National Standards is completely voluntary; their existence does not in any respect preclude anyone, whether he has approved the standards or not, from manufacturing, marketing, purchasing, or using products, processes, or procedures not conforming to the standards.

The American National Standards Institute does not develop standards and will in no circumstances give an interpretation of any American National Standard. Moreover, no person shall have the right or authority to issue an interpretation of an American National Standard in the name of the American National Standards Institute. Requests for interpretations should be addressed to the secretariat or sponsor whose name appears on the title page of this standard.

**CAUTION NOTICE:** This American National Standard may be revised or withdrawn at any time. The procedures of the American National Standards Institute require that action be taken to affirm, revise, or withdraw this standard no later than five years from the date of approval. Purchasers of American National Standards may receive current information on all standards by calling or writing the American National Standards Institute.

Guide to reference and standard ionosphere models/sponsor, American Institute of Aeronautics and Astronautics.

p. cm.

"ANSI/AIAA G-034-1998"

Includes bibliographical references.

ISBN 1-56347-347-X

1. Ionosphere--Mathematical models. I. American Institute of Aeronautics and Astronautics.

QC881.2.I6G85 1999

551.51'45'05118--dc21

99-23533  
CIP

Published by

**American Institute of Aeronautics and Astronautics**

**1801 Alexander Bell Drive, Suite 500, Reston, VA 20191-4344**

Copyright © 1999 American Institute of Aeronautics and Astronautics, Inc.  
All rights reserved.

No part of this publication may be reproduced in any form, in an electronic retrieval system or otherwise, without prior written permission of the publisher.

Printed in the United States of America

# Contents

Foreword .....	v
Summary of Reference and Standard Ionospheres .....	vii

## GLOBAL IONOSPHERE MODELS

USU Time-Dependent Model of the Global Ionosphere, R.W. Schunk and J.J. Sojka .....	1
NCAR Thermosphere-Ionosphere-Electrodynamics General Circulation Model, 1993, R. G. Roble .....	3
Coupled Thermosphere-Ionosphere Model (CTIM), T. J. Fuller-Rowell .....	5
Coupled Thermosphere-Ionosphere-Plasmasphere Model (CTIP), T. J. Fuller-Rowell .....	7
AFRL Global Theoretical Ionospheric Model (GTIM), D. N. Anderson .....	8
Parameterized Ionospheric Model (PIM), D. N. Anderson, R. E. Daniell .....	10
International Reference Ionosphere (IRI), 1996, D. Bilitza .....	12
Empirical Model of the Ionosphere, W. Kohnlein .....	15
The Sheffield University Plasmasphere-Ionosphere Model (SUPIM), G.J. Bailey .....	17
The Field Line Interhemispheric Plasma Model, P. Richards .....	19

## LOWER IONOSPHERE

### D Region:

Algebraic Model, W. Swider .....	21
Numerical Model of D-Region Ion Chemistry, 1995, E. Turunen .....	23

### E Region:

Solar EUV and Chemistry Model, W. Swider .....	26
AFRL Boltzmann-Fokker-Planck Model for the Daytime Lower Ionosphere, J. Jasperse .....	28
AFRL Transport Model for the Electron-Proton-Hydrogen Atom Aurora, J. Jasperse .....	30

## KEY RELATED PROPERTIES

### Electric Fields:

Two-Cell Ionospheric Convection Model, R.A. Heelis .....	33
Heppner-Maynard Electric Field Models, J.P. Heppner and N.C. Maynard .....	35
Millstone Hill Empirical Electric Field Model, 1986, J.C. Foster .....	37
APL High-Latitude Convection Model, M. Ruohoniemi .....	39

### Neutral Winds:

HWM Empirical Wind Model, A. Hedin .....	41
--	----

### Temperature:

Global Empirical Models of $T_e$ , L.H. Brace .....	43
Empirical Model of the Ionospheric Electron and Ion Temperatures, W. Kohnlein .....	45
Photochemical Equilibrium Model for Ionospheric Conductivity, C.E. Rasmussen .....	47
Empirical Model of Conductivities, D. Brautigam .....	48

### Particles and Currents:

Auroral Electron and Ion Fluxes, D. Brautigam .....	50
---	----

**IONOSPHERIC EFFECTS**

**Scintillation—C3I/Navigation Outage:**

WBMOD Ionospheric Scintillation Model (NWRA), 1995,  
E.J. Fremouw and S. Basu ..... 52

**Clutter and Trough—HF/VHF Loss:**

Model of the Trough in the High-Latitude F Layer, J.A. Whalen ..... 55

**TEC—Navigation Errors:**

GPS Eight-Coefficient TEC Model, R.E. Daniell ..... 56  
The CPI TEC Model, R.E. Daniell ..... 57

## Foreword

This *Guide to Reference and Standard Ionosphere Models* has been sponsored by the American Institute of Aeronautics and Astronautics (AIAA) as part of its Standards Program.

The proliferation of ionospheric models and the lack of documentation have hindered general knowledge of their availability as well as their relative strengths, weaknesses, and limitations. The intent of this guide is to compile in one reference practical information about known and available ionospheric models—those that describe the physical properties and practical effects of the ionosphere as a function of altitude, latitude, and other key parameters. At this writing, the included models are those intended for general-purpose, scientific, or aerospace applications and therefore extend to heights ranging from 50 to 10,000 km. Dynamical models of the ionosphere are included in this guide, as the dynamics are essential to many applications.

The guide summarizes the principal features of the models:

- model content
- model uncertainties and limitations
- basis of the model
- database or model input parameters
- publication references
- dates of development, authors, and sponsors
- model codes and sources

The models are grouped according to whether they describe primarily global, regional, or special properties.

There is limited information on standard deviations from the mean values or frequencies of occurrence of some of the variables described by these models. This limits quantitative assessments of uncertainties. Correlation distances for electron densities, and statistics on scintillation are well defined. These and other statistics are discussed in the body of the guide. Candidates for inclusion in this guide have been solicited by means of advertisements in publications including: announcements at national and international meetings of URSI, IAGA, AGU, COSPAR, AIAA, and scientific community newsletters. This collection of models is not exhaustive. It is hoped that future editions will in-

clude additional models from the international community.

The AIAA Standards Procedures provide that all approved Standards, Recommended Practices, and Guides are advisory only. Their use by anyone engaged in industry or trade is entirely voluntary. There is no agreement to adhere to any AIAA standards publication and no commitment to conform to or be guided by any standards report. In formulating, revising, and approving standards publications, the Committees on Standards will not consider patents, which may apply to the subject matter. Prospective users of the publications are responsible for protecting themselves against liability for infringement of patents or copyrights, or both.

We are indebted to those authors who submitted their models for inclusion, to those who offered valuable advice, to Robert S. Skrivanek for notable assistance, and to the reviewers/editors: Drs. Herbert C. Carlson (Chair), David N. Anderson, Santi Basu, Edward J. Fremouw, Roderic A. Heelis, and Robert W. Schunk.

The AIAA Atmospheric & Space Environments Committee on Standards (Shu T. Lai, Chairman) approved the document in April 1999.

The members of this consensus body at the time of voting on the document are:

Dana A. Brewer (NASA Headquarters)  
 Herbert C Carlson (Air Force Office of Scientific Research)  
 Adarsh Deepak (Science & Technology Corp.)  
 Gerald Dittberner (NOAA/NEDIS)  
 L. J. Ehernberger (NASA Ames-Dryden Facility)  
 Jeffrey M. Forbes (University of Colorado)  
 Henry B. Garrett (Jet Propulsion Lab.)  
 G. Barry Hillard (NASA Lewis Research Center)  
 Stuart L. Huston (Boeing Space & Defense)  
 JoAnn Joselyn (NOAA Space Environment Lab.)  
 Neil D. Kelley (National Renewable Energy Lab.)  
 O. Kenneth Moe (USAF Space & Missile Systems Center)  
 Jerry Owens (NASA Marshall Space Flight Center)  
 Robert Sears (Jamieson Science & Engineering)  
 Robert A. Skrivanek (Visidyne Inc.)  
 Guy F. Spitale (Jet Propulsion Laboratory)  
 Walther Spjeldvik (Weber State University)

Robert M. Suggs (NASA Marshall Space Flight  
Center)  
Gopal D. Tejwani (Lockheed Martin Space  
Operations.)  
Alfred Vampola (Consultant)

William W. Vaughan (UAH Research Center)

The AIAA Standards Executive Council ac-  
cepted the document for publication in April  
1999.

## SUMMARY OF REFERENCE AND STANDARD IONOSPHERES

Model (Page #)	Geographic Region	Altitude Range (km)	Parameters	Species Included	Temporal Variation	Output Data Pre- sentation	Principal Application
USU (1)	global	90–1000	$N_e, N_i, T_e,$ $T_{ij}, T_{il}, u_e$ $u_i$	$NO^+, O_2^+, N_2^+$ $N^+, O^+, He^+$	10–100 sec	tables, plots	scientific studies
NCAR/ TIEGCM (3)	global	70–600	$N_e, N_i, N_n,$ $T_e, T_i, T_n,$ $U_e, U_i, U_n$	all ion and neutral	60 sec	tables, plots	scientific studies
CTIM (5)	global	80–10,000	$N_e, N_i$ neutrals $U, V, W$ $T_n, T_e, T_i$	$O^+, H^+, NO^+,$ $O_2, N_2^+, N^+,$ $O, O_2^+, N_2, NO,$ $N(^2D), N(^4S)$	1–6 min	tables, plots	scientific studies
CTIP (7)	global	80–10,000	$N_e, N_i$ neutrals $U, V, W$ $T_n, T_e, T_i, T_e$	$O^+, H^+, NO^+,$ $O_2^+, N_2^+, N^+,$ $O, O_2, N_2, NO,$ $N(^2D), N(^4S)$	1–15 min	tables, plots	scientific studies
GTIM (8)	global	90–22,000	$N_e, N_i$	$NO^+, O_2^+, O^+,$ $H^+, He^+$	diurnal with resolution of 15 min	tables, plots	theoretical climatology and develop- ment of parametric models such as PIM
PIM (10)	global	90–22,000	$N_e, TEC$ $f_oF_2, h_mF_2$ $f_oE, h_mE$	$O^+, NO^+,$ $O_2^+$	diurnal with resolution of 30 min	tables	theoretical climatology, systems design
IRI (12)	global	$N_e$ : 50–2000 $T$ : 120–3000 $N_i$ : 100–2000	$N_e, T_e,$ $T_i, N_i$	$O^+, H^+,$ $He^+, NO^+,$ $O_2^+, N_2^+$ cluster	diurnal (LT, UT, solar zenith angle), seasonal solar cycle	tables, interactive on WWW	spacecraft instrument design, satellite tracking, radio wave propagation, altimeter data analysis ray-tracing, education, etc.
EMI (15)	global coverage (lat)	50–4000	$H^+, He^+,$ $N_2^+, NO^+$	$N^+, O^+,$ $O_2^+, Ne$	diurnal seasonal solar activity	figures, tables	scientific studies
SUPIM (17)	global	90–22,000	$N_e, N_i$ $T_e, T_i$	$O^+, O_2^+$ $NO^+, H^+$ $He^+$	diurnal with resolution of x hr	tables	theoretical studies and climatology
FLIP (19)	mid-lat	90–22,000	$N_e, N_i$ $T_e, T_i$	$H^+, He^+, O^+, N^+$ $NO^+, O_2^+, O(^2D)$ $O(^2P), N(^2D),$ $N(S^4), NO, O(^1D),$ $N_2(vib)$	diurnal 1–30 min resolution	tables, plots	mid-latitude ionosphere- plasma- sphere single ground comparison
ALGEBRAIC (21)	global	60–90		21 positive ions 8 negative ions	diurnal	tables, plots	scientific studies
NUMERICAL CHEM (23)	global	60–90		36 positive ions 19 negative ions	diurnal	tables, plots	scientific studies

## SUMMARY OF REFERENCE AND STANDARD IONOSPHERES

Model (Page #)	Geographic Region	Altitude Range (km)	Parameters	Species Included	Temporal Variation	Output Data Pre- sentation	Principal Application
SOLAR EUV (26)	global	90–120	$N_i^+$ , $N_i^-$ , $N_e$ , neutrals	5 negative ions 4 positive ions	diurnal	tables, plots	scientific studies
SOLAR PHOTO CHEM (28)	mid-lat	100–250	$N_e$ , $N_i$ , $T_e$	$O^+$ , $N_2^+$ , $O_2^+$ , $O$ , $N_2$ , $O_2$ , NO	steady state	tables, plots	mid-latitude daytime E and F1 re- gions of iono- sphere
PROTON ELECTRON AURORAL (30)	high lat >60 deg	90–600	$N_e$ , $N_i$ , $N_2^+$ (3914Å), $N_2$ (3371Å), LBH (1325,1354 1383,1493Å), OI (1356Å), $L\alpha$ (1216Å), H $\beta$ (4861Å), H $\alpha$ (6563Å)	$H^+$ , H O, N <sub>2</sub> , O <sub>2</sub>	steady state	tables, plots	auroral ionosphere: ionization of emission yields
UTD (32)	high lat	150–2000	electrostatic potential	N/A	directly IMF input driven	tables	ionosphere convection flow applications
HEPPNER MAYNARD (35)	high lat >45 deg geomagnetic	100–150	electric potential	N/A	statistical $k_p$ -dependent	point values, plots	modeling studies, comparison to other data
MILL- STONE HILL (37)	high lat	150–2000	electrostatic potential	N/A	either of 3 indices: precipitation, $K_p$ or IMF $B_y/B_z$	tables applications	ionosphere convection flow
APL (39)	global	100–500	$V_i$ (electric potential)	N/A	2 min	velocity maps	scientific modeling studies
HWM (41)	global	7–500	neutral atm wind	total density	diurnal seasonal solar and magnetic activity	tables	wind climatology
EMPIRICAL $T_e$ (43)	global	140–4000	$T_e$ ( $N_e$ dependent)	$T_e$ , $N_e$	latitude local time	tables	climatological model testing
EMPRICAL $T_e$ , $T_i$ (44)	global coverage (lat)	50–4000	$T_e$ , $T_i$	$T_e$ , $T_i$	diurnal seasonal solar activity	figures, tables	scientific studies
PEMIC (45)	high lat	85–220	$N_e$ , $N_i$ , $\sigma_p$ , $\sigma_H$ , $\Sigma_p$ , $\Sigma_H$	$NO^+$ , $O_2^+$ , $N_2^+$ , $O^+$	sec	tables, plots	scientific studies
EMC (48)	high-lat >50 deg geomagnetic	110	$\Sigma_p$ , $\Sigma_H$	$e^-$ ions	hr	tables, figures	input to ionospheric models, scientific studies

## SUMMARY OF REFERENCE AND STANDARD IONOSPHERES

Model (Page #)	Geographic Region	Altitude Range (km)	Parameters	Species Included	Temporal Variation	Output Data Pre- sentation	Principal Application
AEIF (50)	high-lat >50 deg geomagnetic	110	$\Sigma_p, \Sigma_H$	$e^-$ , ions	hr	tables, figures	input to ionospheric models, scientific studies
WBMOD (52)	global	150–1000	plasma irregularity strength & spectrum	$N_e$	diurnal seasonal solar cycle	tables, plots	eng specs, climatology of scintillation at VHF and above
HF/VHF (55)	high lat	F-layer maximum	foF2 MLAT/MLT boundaries	$N_e$	15 min to several hr	graphs, formulae	input to global ionospheric models
GPS TEC (56)	global	N/A	TEC, ionospheric delay at GPS frequencies	N/A	diurnal	tables	single frequency GPS users
CPI TEC (57)	global	N/A	TEC, ionosphere delay at GPS frequencies	$O^+, H^+, He^+$ $NO^+, O_2^+$	diurnal	tables	single frequency GPS users, TEC climatology, TEC variability studies



## USU TIME-DEPENDENT MODEL OF THE GLOBAL IONOSPHERE

### 1. Model content

The USU ionospheric model describes the three-dimensional time-dependent evolution of the global ionosphere at altitudes between 90 and 1000 km. The numerical model yields density distributions for electrons and six ion species ( $\text{NO}^+$ ,  $\text{O}_2^+$ ,  $\text{N}_2^+$ ,  $\text{O}^+$ ,  $\text{N}^+$ ,  $\text{He}^+$ ) as a function of latitude, longitude, and altitude on a prespecified spatial grid. The model also calculates the isotropic electron temperature and the ion temperatures both parallel and perpendicular to the geomagnetic field on the same spatial grid. The model outputs the global density and temperature distributions at specified times.

Numerous physical and chemical processes are contained in the model, including field-aligned diffusion, cross-field electrodynamic drifts, thermospheric winds, polar wind escape, energy-dependent chemical reactions, neutral composition changes, ion production due to EUV radiation and auroral electron precipitation, thermal conduction, diffusion-thermal heat flow, and a host of local heating and cooling mechanisms. The model also takes account of the offset between the geomagnetic and geographic poles.

Depending on the inputs, the global ionospheric model can describe different solar cycle, seasonal, and daily variations. It can describe different levels of sustained geomagnetic activity as well as storm and substorm dynamics.

### 2. Model uncertainties and limitations

**2.1** To a large extent, the reliability of the calculated ionospheric parameters depends on the accuracy to which the global inputs can be specified. The ionospheric model is most sensitive to the magnetospheric electric field and particle precipitation inputs at high latitudes, the thermospheric winds at mid-latitudes, and the equatorial (dynamo) electric fields at low latitudes.

**2.2** The topside plasma scale heights can be significantly affected by the downward electron heat flux through the upper boundary, but this input is virtually unknown on a global scale.

**2.3** Steep spatial gradients can lead to plasma instabilities and scintillations, but the iono-

spheric model does not take instabilities into account.

**2.4** A supercomputer is needed for global simulations.

### 3. Basis of the model

**3.1** The USU model of the global ionosphere is based on an Euler-Lagrange hybrid numerical scheme. For the mid-high latitude region, the ion continuity, momentum, and energy equations are solved as a function of altitude using a fixed spatial grid, whereas for the equatorial region the ion equations are solved along the magnetic field ( $B$ ) from one hemisphere to the conjugate hemisphere on a fixed spatial grid. In all latitudinal domains, the plasma flux tubes are allowed to convect through a moving neutral atmosphere in a direction perpendicular to  $B$  due to magnetospheric, corotational, and dynamo electric fields. The three-dimensional nature of the model is obtained by following many flux tubes of plasma while keeping track of their positions at all times. This approach has the advantage over a purely Eulerian scheme, which requires fixed grid points in latitude and longitude, because more flux tubes can be placed in the high-latitude regions where sharp horizontal gradients are expected, such as near the auroral oval and main trough.

**3.2** The continuity, momentum, and energy equations correspond to a set of nonlinear, second-order, partial differential equations. The equations are first linearized in time, and then finite differences are used for the spatial and temporal derivatives. The resulting coupled algebraic equations are solved with standard matrix inversion techniques.

**3.3** At the lower boundary (90 km), the different ion species are assumed to be in chemical equilibrium, and hence the boundary ion densities are obtained simply by equating local sources and sinks. Likewise, the ion and electron temperatures at the lower boundary are obtained by equating local heating and cooling rates.

**3.4** At the upper boundary (1000 km), a protospheric exchange flux is specified for  $\text{O}^+$ , and the fluxes of the other ion species are assumed to be negligibly small. The upper boundary conditions on the ion and electron temperatures are specifications of the downward heat fluxes through this boundary.

**3.5** A 4-km spatial step is used in the vertical direction, and the time step typically varies from 10 to 100 sec as a given flux tube follows a specified trajectory. The high-latitude region above 500 North is usually modeled with 500 flux tubes of plasma if empirical plasma convection and particle precipitation patterns are used (climatology modeling). For storm and high-resolution studies, 1000–3000 flux tubes are used.

#### **4. Model Input Parameters**

The ionospheric model requires several inputs. The main global inputs are the neutral densities, temperatures, and winds; the magnetospheric and equatorial electric field distributions; the auroral electron precipitation pattern; the downward electron heat flux through the upper boundary; and the protonospheric exchange flux. Typically, empirical or statistical models are used for the required atmospheric and magnetospheric inputs, but in this case the calculated ionospheric parameters pertain to the climatology of the region. For storm and substorm simulations, the temporal variation of the magnetospheric and atmospheric inputs must be specified.

#### **5. Publication References**

**5.1** Schunk, R.W. (1988), "A Mathematical Model of the Middle and High Latitude Ionosphere," *Pure Appl. Geophys.* **127**, 255–303.

**5.2** Sojka, J.J. (1989), "Global Scale, Physical Models of the F Region Ionosphere," *Rev. Geophys.* **27**, 371–403.

#### **6. Dates of Development:**

1973 Original one-dimensional, mid-latitude, multi-ion ( $\text{NO}^+$ ,  $\text{O}_2^+$ ,  $\text{N}_2^+$ ,  $\text{O}^+$ ) model.

1975 High-latitude effects due to plasma convection and particle precipitation added for single plasma flux tubes.

1980 Updated chemical scheme and new ions ( $\text{N}^+$  and  $\text{He}^+$ ) are added.

1981 Plasma convection and particle precipitation patterns added so that multiple flux tubes can be followed.

1982 A more complete ion energy equation is added.

1983 Time-dependent plasma convection and particle precipitation patterns are included so that geomagnetic storms and substorms can be modeled.

1985 An equatorial ionospheric model is added so that the entire globe can be modeled.

1986 The complete electron energy equation is added.

1992 A grid system that allows for a high spatial resolution in a specified region is developed.

#### **7. Model Codes and Sources**

The model is in the form of a large Fortran code, but it is not user friendly and is not available. However, the authors frequently run the model in collaborative studies with both experimentalists and other modelers.

# NCAR THERMOSPHERE- IONOSPHERE-ELECTRODYNAMICS GENERAL CIRCULATION MODEL, 1993

## 1. Model content

The National Center for Atmospheric Research Thermosphere-Ionosphere-Electrodynamics General Circulation Model (TIE-GCM) is a numerical model of the thermosphere and ionosphere that is coupled through self-consistent electrodynamics. The global model is on an effective 5-deg latitude-longitude grid in geographic coordinates and extends in altitude between 95 and 500 km. The model time step is 5 min, and the model runs on the NCAR CRAY Y-MP8-64. The model calculates the global distributions of neutral temperature and winds and also solves for global distributions of the major neutral gas density. The ionospheric portion of the model calculates global distributions of electron density, electron and ion temperature and the number densities of  $O^+(2P)$ ,  $O^+(^2D)$ ,  $O^+(4S)$ ,  $NO^+$ ,  $N_2$ ,  $N^+$ , and  $O_2^+$ . The model also calculates the global distribution of electric fields, currents, and ground magnetic perturbations at each model time step.

The model requires as input a specification of the time-dependent solar EUV and UV flux between 1 and 200 nm, the hemispheric power input of precipitating auroral particles, and the potential drop across magnetic polar caps. It also requires a specification of the amplitude and phase of the diurnal and semi-diurnal components of upward propagating tides from the middle atmosphere. With these time-dependent inputs, the model takes 20 min of NCAR CRAY Y-MP8-64 to simulate one day of coupled thermosphere-ionosphere dynamics.

## 2. Model uncertainties and limitations

**2.1** The model requires an accurate specification of the solar EUV and UV output and its temporal variation, as well as inputs of auroral particle precipitation and cross polar cap potential drop. Various parameterizations of these inputs have been generated and related to solar F107 and F107A indices, as well as Kp and Ap geomagnetic indices. The model auroral inputs can also be specified using the Assimilative Mapping of Ionospheric Electrodynamics input procedure (AMIE) that has been developed at NCAR (Richmond and Kamide, 1988).

**2.2** The model has been used in various satellite track studies, and the accuracy is roughly 10% for total mass density and 5% for temperature.

**2.3** The model is also influenced by tides, gravity waves, and planetary waves that propagate upward from the middle atmosphere and introduce considerable variability into the lower thermosphere. A good description of these features must be specified at the lower boundary of the model.

**2.4** The model requires a specification of initial conditions for time-dependent simulations.

**2.5** This large model has been designed to run only on the NCAR CRAY computer and utilizes the NCAR mass store system to record massive history volumes. Post processors are then used to obtain the desired information such as density along a satellite track or time variations of density and temperature over a given station.

**2.6** The model development is essentially complete, but it is in a constant state of refinement as the details of physical and chemical processes become clearer by existing research.

## 3. Basis of the model

**3.1** The NCAR TIE-GCM is a first-principles model based on nearly 15 years of model development. It does not use any empirical models for the specifications of thermosphere and ionosphere variables but calculates these properties self-consistently. The model solves the primitive equations of dynamic meteorology, but the physical and chemical processes have been adapted to thermospheric heights.

**3.2** The model uses a self-consistent aeronomic scheme based on our current knowledge of the aeronomy of the upper atmosphere and ionosphere.

**3.3** The model is similar to the lower atmosphere general circulation models used to predict meteorology of the lower atmosphere. The numerical procedures are similar, but the TIE-GCM predicts the weather in the upper atmosphere and ionosphere.

## 4. Database

**4.1** There is a set of standard history files for equinox and solstice conditions for solar mini-

mum, solar medium, and solar maximum conditions that are used by the research community for various studies.

**4.2** Most model runs are made on request for a specific geophysical condition. The results are then processed for the specific application using our variety of post processors that have been developed to support the model.

**4.3** The model is being developed as a community model for scientific research but could be developed into an operational model if there is a need.

## **5. Publication references**

**5.1** Dickinson, R.E., E.C. Ridley, and R.G. Roble (1981), "A Three-Dimensional General Circulation Model of the Thermosphere," *J. Geophys. Res.* **86**, 1499–1512.

**5.2** Dickinson, R.E., E.C. Ridley, and R.G. Roble (1984), "Thermospheric General Circulation with Coupled Dynamics and Composition," *J. Atmos. Sci.* **41**, 205–219.

**5.3** Fesen, C.G., R.E. Dickinson, and R.G. Roble (1986), "Simulation of Thermospheric Tides at Equinox with the National Center for Atmospheric Research Thermospheric General Circulation Model," *J. Geophys. Res.* **91**, 4471–4489.

**5.4** Richmond, A.D., and R.G. Roble (1987), "Electrodynamic Effects of Thermospheric Winds from the NCAR Thermospheric General Circulation Model," *J. Geophys. Res.* **92**, 12,365–12,376.

**5.5** Richmond, A.D., and Y. Kamide (1988), "Mapping Electrodynamic Features of the High-Latitude Ionosphere from Localized Observations: Technique," *J. Geophys. Res.* **93**, 5741–5759.

**5.6** Richmond, A.D., E.C. Ridley, and R.G. Roble (1992), "A Thermosphere/Ionosphere General Circulation Model with Coupled Electrodynamics," *Geophys. Res. Letters* **19**, 601-604.

**5.7** Roble, R.G., E.C. Ridley, and R.E. Dickinson (1987), "On the Global Mean Structure of

the Thermosphere," *J. Geophys. Res.* **92**, 8745-8758.

**5.8** Roble, R.G., E.C. Ridley, and R.E. Dickinson (1987), "An Auroral Model for the NCAR Thermospheric General Circulation Model (TGCM)," *Ann. Geophys.* **5A** (6), 369-382.

**5.9** Roble, R.G., E.C. Ridley, and R.E. Dickinson (1982), "Global Circulation and Temperature Structure of the Thermosphere with High Latitude Convection," *J. Geophys. Res.* **87**, 1599-1614.

## **6. Dates of development, authors, and sponsors**

### **6.1 Dates:**

1979 Thermosphere General Circulation Model (TGCM)

1987 Thermosphere-Ionosphere General Circulation Model (TIGCM)

1992 Thermosphere – Ionosphere - Electrodynamics General Circulation Model (TIME-GCM)

1993 Thermosphere–Ionosphere–Mesosphere-Electrodynamics General Circulation Model (TIME-GCM)

**6.2 Authors:** R.G. Roble, E.C. Ridley, A.D. Richmond, and R.E. Dickinson

**6.3 Sponsors:** The National Science Foundation, National Aeronautics and Space Administration, U.S. Air Force, U.S. Navy.

## **7. Model codes and sources**

This research model has been specially designed to run on the NCAR CRAY Y-MPs, and it is not transferable to other machines. Time may be purchased from NCAR to run the model, and the results can be transferred to the requestor's institution for analysis.

## COUPLED THERMOSPHERE-IONOSPHERE MODEL (CTIM)

The coupled thermosphere-ionosphere model (CTIM) has evolved from an integration of a neutral thermospheric code and a high- and mid-latitude ionosphere model. The neutral thermospheric model was originally developed by Fuller-Rowell and Rees (1980) at University College London (UCL); the ionospheric model originated from Sheffield University (Quegan et al., 1982). A complete description is provided in Fuller-Rowell et al. (1996). A recent upgrade of this model, including a self-consistent plasmasphere and low-latitude ionosphere, is described in the section on CTIP.

### 1. Thermosphere model

The thermospheric code simulates the time-dependent structure of the wind vector, temperature, and density of the neutral thermosphere by numerically solving the non-linear primitive equations of momentum, energy, and continuity. The global atmosphere is divided into a series of elements in geographic latitude, longitude, and pressure. Each grid point rotates with Earth to define a noninertial frame of reference in a spherical polar coordinate system. Latitude resolution is 2 deg, and longitude is 18 deg. Each longitude slice sweeps through local time with a 1-min time step. In the vertical direction the atmosphere is divided into 15 levels, in logarithm of pressure, from a lower boundary of 1 Pa at 80 km altitude, to an altitude above 500 km.

The momentum equation is nonlinear, and the solution describes the horizontal and vertical advection, curvature and Coriolis effects, pressure gradients, horizontal and vertical viscosity, and ion drag. The nonlinear energy equation is solved self-consistently with the momentum equation; it describes three-dimensional advection and the exchange between internal, kinetic, and potential energy. The solutions also describe horizontal and vertical heat conduction by both molecular and turbulent diffusion, heating by solar UV and EUV radiation, cooling by infrared radiation, and Joule heating.

Time-dependent major species composition equations are solved including the evolution of O, O<sub>2</sub>, and N<sub>2</sub>, under chemistry, transport and mutual diffusion (Fuller-Rowell et al., 1994). The time-dependent variables of southward and eastward wind, total energy density, and concentrations of

O, O<sub>2</sub>, and N<sub>2</sub> are evaluated at each grid point by an explicit, time-stepping numerical technique. After each iteration the vertical wind, the temperature, the density, and the heights of pressure surfaces are derived. The parameters can be interpolated to fixed heights for comparison with experimental data.

### 2. Ionosphere model

The equations for the neutral thermosphere are solved self-consistently with a high- and mid-latitude ionospheric convection model (Quegan et al., 1982). The ionosphere is computed self-consistently with the thermosphere poleward of 23-deg latitude in both hemispheres. In this coupled model the ionospheric Lagrangian frame has been modified to be more compatible with the Eulerian frame by the use of semi-Lagrangian technique (Fuller-Rowell et al. 1987, 1988).

Transport under the influence of the magnetospheric electric field is explicitly treated, assuming  $\mathbf{E} \times \mathbf{B}$  drifts and collisions with the neutral particles. The densities of atomic ions H<sup>+</sup> and O<sup>+</sup> and the ion temperature are evaluated over the height range from 100 to 10,000 km, including horizontal transport, vertical diffusion, and the ion-ion and ion-neutral chemical processes. Below 400 km, the additional contribution from the molecular ion species N<sub>2</sub><sup>+</sup>, O<sub>2</sub><sup>+</sup>, and NO<sup>+</sup> and atomic ion N<sup>+</sup> are included. The ion temperature is calculated under the assumption of thermal balance between heat gained from the electron gas and from ion-neutral frictional heating, and heat lost to the neutral gas.

### 3. Common inputs

The magnetospheric input to the model is based on the statistical models of auroral precipitation and electric fields described by Fuller-Rowell and Evans (1987) and Foster et al. (1986), respectively. Both inputs are keyed to a hemispheric power index (PI), based on the TIROS/NOAA auroral particle measurements, and are mutually consistent in this respect. The PI index runs from 1 to 10 to cover very quiet to storm levels of geomagnetic activity; the relationship between PI and K<sub>p</sub> can be found in Foster et al. (1986). Alternative electric field and auroral precipitation models can easily be incorporated into the model.

The (2,2), (2,3), (2,4), (2,5), and (1,1) propagating tidal modes are imposed at 97 km altitude (Fuller-Rowell et al. 1991); amplitude and phase can be prescribed. Ionization rates from the EUV flux are evaluated from reference spectra for high

and low solar activity on the basis of the Atmospheric Explorer (AE) measurements.

#### 4. Publication references

4.1 Foster, J.C., J.M. Holt, R.G. Musgrove, and D.S. Evans (1986), *Geophys. Res. Letters* **13**, 656–659.

4.2 Fuller-Rowell, T.J., and D.S. Evans (1987), *J. Geophys. Res.* **92**, 7606–7618.

4.3 Fuller-Rowell, T.J., and D. Rees (1980), *J. Atmos. Sci.* **37**, 2545–2567.

4.4 Fuller-Rowell, T.J., S. Quegan, D. Rees, R.J. Moffett, and G.J. Bailey, *J. Geophys. Res.* **92**, 7744–7748, 1987.

4.5 Fuller-Rowell, T.J., S. Quegan, D. Rees, R.J. Moffett, and G.J. Bailey (1988), *Pure Appl. Geophys.* **127**, 189–217.

4.6 Fuller-Rowell, T.J., D. Rees, H.F. Parish, T.S. Viridi, P.J.S. Williams, and R.G. Johnson (1991), *J. Geophys. Res.* **96**, 1181–1202.

4.7 Fuller-Rowell, T.J., M.V. Codrescu, R.J. Moffett, and S. Quegan (1994), *J. Geophys. Res.* **99**, 3893–3914.

4.8 Fuller-Rowell, T.J., D. Rees, S. Quegan, R.J. Moffett, M.V. Codrescu, and G.H. Millward (1996), *STEP Handbook of Ionospheric Models*, edited by R.W. Schunk, Utah State Univ.

4.9 Quegan, S., G.J. Bailey, R.J. Moffett, R.A. Heelis, T.J. Fuller-Rowell, D. Rees, and R.W. Spiro (1982), *J. Atmos. Terr. Phys.* **44**, 619–640.

#### 5. Contacts

The model is available for collaborations. Please contact Tim Fuller-Rowell, Space Environment Center, 325 Broadway, Boulder, CO 80303, tel. 303/497-5764 (e-mail [tjfr@sel.noaa.gov](mailto:tjfr@sel.noaa.gov)); or Mikhail Codrescu, same address, tel. 303/497-6763 (e-mail [codrescu@sel.noaa.gov](mailto:codrescu@sel.noaa.gov)).

## COUPLED THERMOSPHERE- IONOSPHERE-PLASMASPHERE MODEL (CTIP)

### 1. Model content

The Coupled Thermosphere-Ionosphere-Plasmasphere model (CTIP) is an enhanced version of the CTIM model described elsewhere in this guide. The new enhanced version is identical to CTIM but includes a fully coupled model of the Earth's mid- and low-latitude ionosphere and plasmasphere, where CTIM relies on an empirical description.

### 2. Basis of the model

The new ionosphere-plasmasphere component of CTIP solves the coupled equations of continuity, momentum and energy to calculate the densities, field-aligned velocities and temperatures of the ions  $O^+$  and  $H^+$  and the electrons, along a total of 800 independent flux-tubes arranged in magnetic longitude and L value (20 longitudes and 40 L values). The effects of  $\mathbf{E} \times \mathbf{B}$  drift at lower latitudes are incorporated by the inclusion of an empirical low-latitude electric field model. Full three-dimensional routines are used to interpolate parameters between the thermosphere and ionosphere-plasmasphere grids.

Recent developments of the CTIP model have included changing the mid- and low-latitude ionosphere/plasmasphere component such that the basic equations are now solved in a Eulerian (rather than Lagrangian) framework. This is a subtle change that allows ionospheric  $\mathbf{E} \times \mathbf{B}$  convection to take any form (previous incarnations required flux-tubes to return to their geographic starting positions during a 24-hr simulation). In addition the resolution of the ionosphere, in the height-latitude plane, has been significantly in-

creased such that the equatorial ionosphere, between altitudes of 200 and 1300 km, is modeled with a vertical resolution of 20 km. The new resolution represents a threefold increase in the number of individual flux-tubes solved within the model, necessary in order to correctly simulate (in particular) the dusk sector ionospheric response to the "pre-reversal enhancement" low-latitude electric field.

The CTIP model is thus a fully dynamic coupled model of the global thermosphere and ionosphere and has recently been used to study the mid-latitude ionospheric F2-layer annual and semi-annual variations (Millward et al., 1996a). A full description of the mathematical basis of the model has been given by Millward et al. (1996b).

### 3. Publication references

**3.1** Millward, G.H., H. Rishbeth, T.J. Fuller-Rowell, A.D. Aylward, S. Quegan, and R.J. Moffett (1996a), "Ionospheric F2-Layer Annual and Semi-Annual Variations," *J. Geophys. Res.* **101** (3).

**3.2** Millward, G.H., R.J. Moffett, S. Quegan, and T.J. Fuller-Rowell (1996b), "A Coupled Thermosphere-Ionosphere-Plasmasphere Model, CTIP," *STEP Handbook of Ionospheric Models*, edited by R.W. Schunk, Utah State Univ.

### 4. Model codes and sources

The model consists of a large and tortuous FORTRAN code, requires a powerful workstation or supercomputer to run, and is not particularly user-friendly. However, it is suitable for collaborative studies. Contact either Tim Fuller-Rowell (at the address given in the CTIM report) or George Millward, Space Environment Center, 325 Broadway, Boulder, CO 80303, tel. 303/497-7754 (e-mail gmillward@sel.noaa.gov).

## AFRL GLOBAL THEORETICAL IONOSPHERIC MODEL (GTIM)

### 1. Model content

The Air Force Research Laboratory (AFRL) Global Theoretical Ionospheric Model (GTIM) is a time-dependent, ionospheric model that calculates ion ( $\text{NO}^+$ ,  $\text{O}_2^+$ ,  $\text{O}^+$ ,  $\text{He}^+$ ,  $\text{H}^+$ ) densities as a function of altitude, latitude, longitude and local time, globally. The output from GTIM covers the height range from 90 to 1600 km on a prespecified grid of latitudes and longitudes, depending on the scale of the phenomenon under investigation. Nominally, the output ion and electron densities are calculated every 2 deg dip latitude, every 5 deg longitude, and every 0.5 hr local time.

The model calculates  $\text{O}^+$ ,  $\text{He}^+$ , and  $\text{H}^+$  densities by solving the coupled ion momentum and continuity equations numerically using a Crank-Nicholson implicit finite differencing technique. The model includes the effects of production by solar EUV radiation and energetic particle precipitation, loss through charge exchange with the neutral atmosphere and transport by  $\mathbf{E} \times \mathbf{B}$  drift, ambipolar diffusion, and collisions with neutral atmosphere. The offset between the geographic poles and geomagnetic poles is taken into account. The molecular ions  $\text{NO}^+$  and  $\text{O}_2^+$  are calculated under the chemical equilibrium assumption that production equals loss, and no transport effects are included.

### 2. Model uncertainties and limitations

In calculating global ion and electron density distributions, the model uncertainties relate to how well the required inputs to GTIM can be specified. A number of studies have established that, if these can be realistically specified, then excellent agreement between calculated and observed electron density profiles is achieved. At low and high latitudes, the most important transport mechanism is  $\mathbf{E} \times \mathbf{B}$  drift whereas at mid latitudes, it is neutral winds that are critical in determining realistic ion and electron densities.

The major limitation of the model is that it is not coupled to the neutral atmosphere, the electrodynamics, or the energetics of the plasma so that neither temperatures nor electric fields are self-consistently calculated.

### 3. Basis of the model

GTIM solves the coupled ion ( $\text{O}^+$ ,  $\text{He}^+$ , and  $\text{H}^+$ ) momentum and continuity equations in a frame of reference that drifts with the  $\mathbf{E} \times \mathbf{B}$  drift velocity (Eulerian frame of reference) of the ion and electrons. The  $r$ ,  $q$ ,  $f$  coordinate system is transformed to an  $\alpha$ ,  $\beta$ ,  $\gamma$  coordinate system, where  $\alpha$  and  $\beta$  are perpendicular to the geomagnetic field line direction, and  $\gamma$  is parallel to  $\mathbf{B}$ . A number of transformations are carried out which facilitate the solving of the linear, second-order partial differential equation. At low and mid latitudes the solution is carried out along the entire field line from one hemisphere (90 km N) to the other (90 km S), and the boundary conditions at both ends assume  $[\text{O}^+] = 0$ . At high latitudes (above about  $\pm 60$  deg dip latitude), the upper boundary condition at 1600 km provides flux values ( $Nv_z$ ) parallel to  $\mathbf{B}$ .

### 4. Model input parameters

Inputs to GTIM include a neutral atmosphere model, a solar production rate model,  $\mathbf{E} \times \mathbf{B}$  drift pattern, a model for precipitating energetic electrons and protons, a horizontal neutral wind model, and a model for electron and ion temperatures. All of these inputs come from well established references and observations and will not be detailed here.

### 5. Publication references

5.1 Anderson, D.N. (1973), "A Theoretical Study of the Ionospheric F Region Equatorial Anomaly, I; Theory," *Planetary Space Sci.* **21**, 409–420.

5.2 Decker, D.T., C.E. Valladares, R. Sheehan, S. Basu, D.N. Anderson, and R.A. Heelis (1994), "Modeling Daytime F Layer Patches over Sondrestrom," *Radio Sci.* **29**, 249–268.

### 6. Dates of development, authors, and sponsors

#### 6.1 Dates:

1973 Development of the low-latitude portion of GTIM).

1976 Development of the mid-latitude portion of GTIM).

1994 Development of the high-latitude portion of GTIM).

1995–97 Addition of light ions ( $\text{He}^+$  and  $\text{H}^+$ ) to low- and mid-latitude portion of GTIM.

**6.2 Authors:** D.N. Anderson, D.T. Decker, M.W. Fox, R.E. Daniell, and R.W. Simon.

## **7. Model codes and sources**

The model consists of a large number of Fortran coded subroutines that provide the GTIM output, but in no way is it well documented, user-friendly, or available to outside users. However, many collaborative studies have been carried out using GTIM.

## PARAMETERIZED IONOSPHERIC MODEL (PIM)

### 1. Model content

The Parameterized Ionospheric Model (PIM) is a global model of the *theoretical* climatology of the ionosphere. That is, PIM is a parameterization of the output from an amalgamation of theoretical ionospheric models, including the USU Time Dependent Ionospheric Model (TDIM) for high latitudes and the Global Theoretical Ionospheric Model (GTIM) for low and mid latitudes, augmented by the empirical plasmasphere model of Gallagher (1988). An earlier version of PIM has been described by Daniell et al. (1995).

The output from all of these models has been parameterized in terms of solar activity ( $F_{10.7}$ ), geomagnetic activity ( $K_p$ ), and season (Equinox, June Solstice, December Solstice). The format of the output of PIM is user selectable, and includes electron density profiles and/or profile parameters (TEC,  $N_mF_2$ ,  $h_mF_2$ ,  $N_mE$ ,  $h_mE$ , etc.) on user-specified grids in latitude/longitude/altitude (geographic or geomagnetic) or azimuth/elevation/range.

### 2. Model uncertainties and limitations

PIM is a climatological model based on diurnally reproducible runs of physics-based models. As such, it cannot accurately reproduce specific situations, especially the storm-time ionosphere. It is intended to represent "typical" (rather than "average") ionospheric conditions.

Because the model is based on seasonal runs, it does not represent the complete annual variation of the ionosphere and is most inaccurate between equinoxes and solstices.

### 3. Basis of the model

PIM consists of two major components: (1) a large set of coefficient files, from which the electron density profile may be derived at any specified latitude, longitude, season, and solar geophysical condition, and (2) an algorithm for reconstructing the electron density profiles from these coefficients.

PIM is based on diurnally reproducible runs of its parent physics-based models for specified solar/geophysical conditions and seasons. That is, the physics-based models are run with constant or

steady-state forcing functions until the steady-state response of the ionosphere is obtained. (This usually occurs after a few hours of solar illumination.) The output of the physics-based models consists of altitude profiles of the densities of the three dominant ions of the E and F regions ( $O^+$ ,  $N_2^+$ , and  $O_2^+$ ) on a latitude/longitude grid at regular intervals of local time or UT, depending on the model.

The ion density profiles are then represented as linear combinations of Empirical Orthonormal Functions (EOFs), which are derived from the complete set of profiles for a given set of solar/geophysical conditions. Depending on latitude region, the coefficients of the EOFs are fit by orthogonal functions in latitude, longitude, and/or UT.

The resulting coefficients are stored in files and constitute one of the two major constituents of PIM. The other component, the FORTRAN code itself, reconstructs the ion density profiles at the times and places specified by the user and sums the ion densities to obtain the electron density. If the user has asked for profile parameters, the height and density of the E- and F-layer peaks are found, and the profile is integrated to produce TEC.

The structure of the coefficient files differs for the various ionospheric regions. Merging between regions is accomplished by averaging between profiles in overlapping regions. Interpolation for solar/geophysical conditions between the values of the model runs is also accomplished by operating on profiles (rather than coefficients). This is because the EOFs were derived separately from each block of runs; that is, the basis functions are different for different sets of solar/geophysical conditions and different ionospheric regions.

This will probably change in PIM version 2, which will be based on a "universal" set of EOFs so that all interpolation can be done in "coefficient space." It will also be based on a single, unified ionospheric model, GTIM.

### 4. Model input parameters

The user inputs are the date and time (UT) of the run, the solar/geophysical conditions ( $F_{10.7}$  and  $K_p$ ), choice of coordinates (geomagnetic or geographic), choice of output grid (latitude/longitude/altitude or azimuth/elevation/range), and the specifics of the output grid.

## 5. Publications references

**5.1** Daniell, R.E., L.D. Brown, D.N. Anderson, M.W. Fox, P.H. Doherty, D.T. Decker, J.J. Sojka, and R.W. Schunk (1995), "Parameterized Ionospheric Model: A Global Ionospheric Parameterization Based on First Principles Models," *Radio Sci.* **30**, 1499–1510.

**5.2** Gallagher, D.L., P.D. Craven, and R.H. Comfort (1988), "An Empirical Model of the Earth's Plasmasphere," *Adv. Space Res.* **8**, 15–24.

## 6. Dates of development, authors, and sponsors

### 6.1 Dates:

1987–90 Development of the high-latitude portion of the model.

1990 Development of the low- and mid-latitude portion.

1993 Version 1 of PIM.

1997 Most recent version of the code (1.6).

**6.2 Authors:** R.E. Daniell, L.D. Brown, W.G. Whartenby, J.J. Sojka, P.H. Doherty, D.T. Decker, and D.N. Anderson.

**6.3 Sponsor:** Air Force Research Laboratory.

## 7. Model codes and sources

The model may be obtained by contacting Lincoln Brown at CPI, tel. 781/487-2250 (e-mail [brown@cpiboston.com](mailto:brown@cpiboston.com)). The source code and associated coefficient files are available free of charge from either of two ftp sites on the Internet. They are also available on CD-ROM for a nominal charge. (Contact Mr. Brown for specific information.) The source code is FORTRAN, and each version is verified to run under MS-DOS, DEC-VMS, and Sun-UNIX operating systems. (With minor modifications, the code has been successfully run under other UNIX "flavors.") There are approximately 40–50 registered PIM users around the world.

## INTERNATIONAL REFERENCE IONOSPHERE (IRI), 1996

### 1. Model content

The International Reference Ionosphere is the standard ionospheric model recommended for international use by the scientific unions Committee on Space Research (COSPAR) and International Union of Radio Science (URSI). A joint Working Group of COSPAR and URSI is in charge of developing and improving the model. By charter IRI, like other international standard models (e.g., CIRA, MSIS, IGRF), is an empirical model, thus avoiding the uncertainties of the evolving theoretical understanding. Annual IRI Workshops are the forum for progress/status reports of ongoing IRI projects, for comparisons with new data sources, for resolving issues of conflicting data sources, and for decisions about improvements and additions for the next release of the model. The presentations from these workshops are published in *Advances in Space Research*, Vols. (Nos.) **4** (1), **5** (7), **5** (10), **7** (6), **8** (4), **10** (8), **10** (11), **11** (10), **13** (3), **14** (12), **15** (2), **16** (1).

IRI provides monthly averages of the electron density, the ion composition ( $O^+$ ,  $H^+$ ,  $He^+$ ,  $NO^+$ ,  $O_2^+$ ,  $N_2^+$ , cluster ions), the electron temperature, and the ion temperature for magnetically quiet conditions. Efforts are underway to include models for ionospheric storm effects and models for the ion drift and spread-F.

The IRI model, its background, database, and mathematical formulas are explained in detail in special reports published by URSI (Rawer et al., 1978), by the WDC-A-STP (Rawer et al., 1981), and by the NSSDC (Bilitza, 1990).

### 2. Model uncertainties and limitations

Like any empirical model, IRI is as good and representative as the data that are available for developing/improving the model. Since most of the ionospheric data have been accumulated at European and North American latitudes, these regions are also the ones that are best represented in IRI. The Northern hemisphere and the continents in general are better represented than the Southern hemisphere and the oceans, again because of obvious differences in data volume. The IRI model should be primarily used for sub-auroral latitudes. At auroral and polar latitudes, the model has to rely on data from just a few sta-

tion and satellites, clearly not enough to fully describe this highly variable region. At these high latitudes, IRI should be considered as a first estimate for describing the background ionosphere.

The uncertainties are typically as follows:

	Peak height	Peak density	Temperatures	Ion comp.
F region	±15%	±30%	±20%	±50%
E region	±5%	±10%	±10%	±50%
D region	±10%	±70%		

Improvements in the accuracy of the electron density values can be obtained by introducing measured values for the F peak height and density; IRI supports this option. In addition, IRI provides an option to use measured electron densities to obtain more accurate electron temperatures by employing the well known anti-correlation between electron temperature and density.

### 3. Basis of the model

The IRI electron density model uses the CCIR world maps for the F and E peak parameters. A special formula was developed by the IRI team to convert the CCIR-given M3000 propagation factor to the F peak height. For the F peak density an additional choice is given with the URSI-88 maps. These were developed by a special URSI Working Group (C. Rush, Chair) and have shown better results than CCIR in the ocean areas. In addition, a user can also enter measured peak parameters into IRI, if available. The CCIR formulas for the F1 ledge and the E peak densities were modified for IRI to better agree with more recent measurements. The IRI topside is based on an analytical representation of Bent's compilation of Alouette and ISIS topside sounder data. Incoherent scatter data from Jicamarca and Arecibo and AEROS and AE-C *in situ* measurements have been used to improve the formula at low latitudes. The representation of the region between E and F peaks is based on ionosonde real-height profiles and on incoherent scatter data (valley). The D-region model assumes an inflection point at 80 to 88 km; this height is correlated to the transition from molecular to cluster ions. The global and temporal variation of the density at that point was modeled with the help of all available (reliable) rocket data.

The electron and ion temperature models are based largely on AEROS RPA and AE-C, ISIS-1, ISIS-2 Langmuir probe data. These data provide a global mapping of temperatures at several alti-

tudes. The whole profile was then established with the help of incoherent scatter data from Jicamarca, Arecibo, and Millstone Hill. At 120 km, the plasma temperatures coincide with the value given by the COSPAR International Reference Atmosphere (CIRA); this was one of the COSPAR requirements. Through all altitudes the temperatures are such that  $T_n < T_i < T_e$ .

The IRI ion composition model assumes charge neutrality. IRI primarily models the global and temporal variation of atomic and molecular oxygen ions ( $O^+$ ,  $O_2^+$ ) and then fills up to 100% with light ions ( $H^+$ ,  $He^+$ ) above the F peak and with  $NO^+$  ions below. The model is based on a compilation of rocket and satellite RPA and IMS data. The rather limited database makes the ion composition model the weakest part of the IRI. Problems with instrument calibrations have made it difficult to use IMS data from several of the early satellites. Discrepancies were also found between satellite and incoherent scatter measurements. Efforts are now focussing on using the transition heights (light ions to  $O^+$ ,  $O^+$  to molecular ions, molecular to cluster, cluster to negative ions) as the characteristic parameters of the composition profiles.

#### 4. Database

Electron density: ionosonde (E,F peak, bottom-side), incoherent scatter radar (hmF2, E-valley, topside), absorption (D-region), rockets (D-, E-region), Alouette, ISIS topside sounder (topside), AEROS, AE-C, DE-2 *in situ* (topside); ion composition: RPA and IMS measurements from satellites (AE-C, AEROS-B, S3-1, OGO-6, Electron 2, 4, Cosmos 274, Sputnik 3) and rockets; temperatures: Langmuir probe and RPA measurements from AEROS-A,B, ISIS-1,-2, AE-C, -E, DE-2, incoherent scatter data from Jicamarca, Arecibo, Millstone Hill, St. Santin, Malvern.

#### 5. Publication references

**5.1** Bilitza, D. (1990), "International Reference Ionosphere 1990," NSSDC/WDC-A-R&S 90-22, Greenbelt, MD.

**5.2** Bilitza, D.,K., and E.G. Rawer, eds. (1994), "Ionospheric Models," *Adv. Space Res.* **14** (12).

**5.3** Rawer, K., S. Ramakrishnan, and D. Bilitza

(1978), "International Reference Ionosphere 1978," URSI Special Rept., Brussels, Belgium.

**5.4** Rawer, K., D. Bilitza, and S. Ramakrishnan (1978), "Goals and Status of the International Reference Ionosphere," *Rev. Geophys.* **16**, 177–181.

**5.5** Rawer, K., J.V. Lincoln, and R.O. Conkright (1981), "International Reference Ionosphere IRI-79," WDC-A-STP Rept. UAG-82, Boulder, CO.

**5.6** Rawer, K., and W.R. Piggott (1990), "Development of IRI-90," *Adv. Space Res.* **10** (11).

**5.7** Rawer, K., and W.R. Piggott (1991), "Enlarged Space and Ground Data Base for Ionospheric Modelling," *Adv. Space Res.* **11** (10).

**5.8** Rawer, K., W.R. Piggott, and A.K. Paul (1993), "Advances in Global/Regional Descriptions of Ionospheric Parameters," *Adv. Space Res.* **13** (3).

**5.9** Rawer, K., W.R. Piggott, and A.K. Paul, eds. (1995), "Off Median Phenomena and IRI," *Adv. Space Res.* **15** (2).

**5.10** Rawer, K., D. Bilitza, and W. Singer, eds. (1995), "The High Latitudes in the IRI," *Adv. Space Res.* **16** (1).

**5.11** Rawer, K., D. Bilitza, K. Mahajan, and A. Mitra, eds. (1996), "Low and Equatorial Latitudes in the IRI," *Adv. Space Res.* **18** (6).

#### 6. Dates of development, authors, and sponsors

##### 6.1 Dates:

- 1968 Working Group established.
- 1972 First set of preliminary tables.
- 1978 IRI-78, URSI Special Report.
- 1981 IRI-80, WDC-A-STP Report UAG-82.
- 1986 IRI-86 (also on diskette for use on PCs).
- 1990 IRI-90, NSSDC Report 90-22.
- 1995 IRI-95, anonymous ftp and WWW.

**6.2 Authors:** COSPAR/URSI Working Group (K. Rawer, L. Bossy, and D. Bilitza, Chairs).

#### 7. Model codes and sources

The model codes can be retrieved from the anonymous ftp site at [nssdca.gsfc.nasa.gov](http://nssdca.gsfc.nasa.gov) in directory `pub/models/IRI`; an ASCII version of the model coefficients can be found in directory `pub/models/IRI90ASCII`. The software package can be also obtained on diskette from NSSDC's request coordination office (CRUSO), National Space Science Data Center, NASA/GSFC, Code

633.4, Greenbelt, MD 20771, tel. 301/286-6695, FAX 301/286-1771 (e-mail [request@nssdca.gsfc.nasa.gov](mailto:request@nssdca.gsfc.nasa.gov)). The model can also be accessed and run interactively on the World Wide Web at <http://nssdc.gsfc.nasa.gov/space/model>. There are also WWW pages describing the model and listing the Working Group composition and the IRI Workshops that have been held so far.

## EMPIRICAL MODEL OF THE IONOSPHERE

### 1. Model content

The empirical model of the ionosphere provides number densities ( $\text{cm}^{-3}$ ) of

Atomic ions:	$\text{H}^+, \text{He}^+, \text{N}^+, \text{O}^+$
Molecular ions:	$\text{N}_2^+, \text{NO}^+, \text{O}_2^+$
Electrons:	$\text{N}_e$

as a function of

Altitude:	50–4000 km
Latitude:	dipole latitude, $\text{N}_2$ , $\text{O}_2$ , $\text{O}$ , $\text{NO}$
Time:	day count $d$ (annual variation) magnetic local time $\tau$
Solar activity:	solar flux $F_{10.7}$ for quiet geophysical conditions ( $K_p \leq 3$ )

The number densities  $n$  of the ion species and the electrons are obtained from the appropriate figures (Köhnlein, 1989a and 1989b). At  $F_{10.7} = 84 \times 10^{-22} \text{ Wm}^{-2} \text{ Hz}^{-1}$  and  $K_p \leq 3$ :

Average density (time independent):  
see Köhnlein (1989a and 1989b, Figs. 3–6),  
 $\log_{10}n$  vs altitude;

Time-independent density (latitudinal):  
see Köhnlein (1989a and 1989b, Figs. 7–18),  
 $\log_{10}n$  vs altitude at  $f = 90^\circ, 45^\circ, 0^\circ, -90^\circ$ ;  
 $\log_{10}n$  vs dipole latitude at discrete heights;

Annual variation:  
see Köhnlein (1989a and 1989b, Figs. 19–30),  
 $\log_{10}n$  vs altitude at equinox and solstice  
conditions ( $d = 80, 173, 266, 356$ );  
comparison with data:  
 $\log_{10}n$  vs day count at discrete heights;  
 $\Delta \log_{10}n(\text{relative})$ :  
dipole latitude vs day count at discrete  
heights;

Diurnal variation:  
see Köhnlein (1989a, Figs. 31–46), and  
Köhnlein (1989b, Figs. 31–48),  
 $\log_{10}n$  vs altitude at  $f = 0^\circ, 45^\circ$ , and  $t =$   
0h, 6h, 12h, 18h;  
comparison with data:

$\log_{10}n$  vs magnetic local time at discrete  
heights and  $f = 0^\circ, 45^\circ$ ;

$\Delta \log_{10}n(\text{relative})$ :  
dipole latitude vs magnetic local time at dis-  
crete heights;

And superpositions thereof, i.e.,

diurnal variation + relative annual variation  
 $\Rightarrow$  diurnal variation at a selected day of the  
year;  
annual variation + relative diurnal variation  
 $\Rightarrow$  diurnal variation at a selected magnetic  
local time.

### 2. Model uncertainties and limitations

The discrepancies between the model and the observations (used) are shown for the annual and diurnal variations in Köhnlein (1989a and 1989b, Figs. 20, 23, 26, 29, 32, 33, 36, 37, 40, 41, 44, 45), and in Köhnlein (1989b, Figs. 46 and 47). In general, the model agrees well with the observations.

The uncertainties of the model are mainly due to the uneven data coverage and the simplicity of the analytical approach (e.g., linearity, no longitudinal terms, no disturbed conditions).

Data from epochs not used in the database may show greater deviations from the model. This is especially true for disturbed geophysical conditions that are not considered in the model (also see Köhnlein, 1993).

### 3. Basis of the model

The vertical and horizontal structures of the model are treated on an equal footing.

The plasma parameters are expanded into spherical harmonics (Köhnlein, 1989a, Eqs. 2.1–2.10) wherein the model coefficients depend on altitude, solar flux  $F_{10.7}$ , and the geomagnetic index  $K_p$ .

Restricting the model to quiet geophysical conditions ( $K_p \leq 3$ ), the above coefficients depend linearly on  $F_{10.7}$ , whereas their height variations are expressed by cubic spline functions.

### 4. Database

The database of the model consists of observations by satellites, incoherent scatter stations, and rocket profiles covering the time interval 1964–1979 (Köhnlein, 1989a, Table1; and Köhnlein,

79 (Köhnlein, 1989a, Table1; and Köhnlein, 1989b, Table1 and Figs.1 and 2).

## 5. Publication references

**5.1** Köhnlein, W. (1989a), "A Model of the Terrestrial Ionosphere in the Altitude Interval 50–4000 km: I. Atomic Ions ( $H^+$ ,  $He^+$ ,  $N^+$ ,  $O^+$ )," *Earth, Moon, and Planets* **45**, 53–100.

**5.2** Köhnlein, W. (1989b), "A Model of the Terrestrial Ionosphere in the Altitude Interval 50–4000 km: II. Molecular Ions ( $N_2^+$ ,  $NO^+$ ,  $O_2^+$ ) and Electron Density," *Earth, Moon, and Planets* **47**, 109–163.

**5.3** Köhnlein, W. (1993), "Comparison of the Ion Composition Data with Empirical Models (Comment)," *Advances in Space Research* **13** (3), 85–86, 125–132.

## 6. Dates of development, authors, and sponsors

**6.1 Date:** 1983.

**6.2 Author:** W. Köhnlein.

**6.3 Sponsors:** Deutsche Forschungsgemeinschaft and University of Bonn.

## 7. Model codes and sources

The model was developed in FORTRAN code specifically adapted to a CDC computer.

Because of the detailed graphical representation, Köhnlein (1989a and 1989b) can be used as a quick reference for ion and electron densities at low solar fluxes ( $F_{10.7} \approx 84$ ) and quiet geophysical conditions ( $K_p \leq 3$ ) in the altitude interval 50–4000 km.

# THE SHEFFIELD UNIVERSITY PLASMASPHERE-IONOSPHERE MODEL (SUPIM)

## 1. Model content

The Sheffield University Plasmasphere-Ionosphere Model (SUPIM) is a mathematical model that describes the distribution of ionization within the Earth's mid and equatorial latitude ionosphere. In the model, time-dependent equations of continuity, momentum, and energy balance for the  $O^+$ ,  $H^+$ ,  $He^+$ ,  $N_2^+$ ,  $O_2^+$  and  $NO^+$  ions, and the electrons, are solved along magnetic field lines for the ion and electron concentrations, field-aligned velocities, and temperatures. The magnetic field is an eccentric-dipole representation of the Earth's magnetic field, the offset between the magnetic and geographic poles being determined from the first eight non-zero terms of the usual spherical harmonic expansion of the geomagnetic scalar potential used in the International Geomagnetic Reference Field (IGRF). Particularly cases of the eccentric dipole are the tilted-centered dipole and the axial-centered dipole. These cases are obtained by truncating the spherical harmonic expansion after the first three nonzero terms and the first term, respectively.

Included in the model are numerous physical and chemical processes. The principal processes include ion production due to solar EUV radiation, ion production and loss due to chemical reactions between the constituent ions and with the neutral gases, ambipolar and thermal diffusion, ion-ion and ion-neutral collisions, thermospheric meridional and zonal winds, electrodynamic drift, thermal conduction, photoelectron heating, frictional heating, and a host of local heating and cooling mechanisms.

Enhancements/modifications have been made to the "standard" model for specific studies. For example, inclusion of sub-auroral ion drifts (SAIDs), a self-consistent low-latitude atmospheric dynamo model, anisotropic ion temperatures, vibrational excitation of  $N_2$ , the separation of  $O^+$  into its  $^4S$ ,  $^2D$  and  $^2P$  states, and vertical neutral winds.

Depending upon the inputs the model can describe different solar cycle, seasonal, daily, and magnetic activity variations. It can also provide descriptions of the diurnal, altitude, latitude, and longitudinal variations.

## 2. Model uncertainties and limitations

**2.1** To a large extent, the reliability of the calculated ionospheric parameters depends upon the accuracy to which the model inputs can be specified.

**2.2** Except for a few locations, the model inputs of thermospheric wind and the vertical  $\mathbf{E} \times \mathbf{B}$  drift are poorly known. Some adjustments to these parameters may be needed.

## 3. Basis of the model

**3.1** The model is a mathematical formulation of the known physical and chemical processes of the Earth's ionosphere and plasmasphere. The motion of the plasma is considered to be due to ambipolar diffusion parallel to the magnetic field with an additional  $\mathbf{E} \times \mathbf{B}$  drift perpendicular to the magnetic field.

**3.2** The model equations are solved at a discrete set of points along an eccentric dipole magnetic field line from a base altitude of around 120 km in the northern hemisphere to a base altitude of around 120 km in the southern hemisphere. There are switches in the model code to make the magnetic field a tilted-centered or axial-centered dipole.

**3.3** At mid latitudes, the vertical  $\mathbf{E} \times \mathbf{B}$  drift velocity has little effect on the model results and is usually taken to be zero. For many applications, only one field line needs to be considered.

**3.4** At equatorial latitudes, inclusion of the vertical  $\mathbf{E} \times \mathbf{B}$  drift is essential as this drift gives rise to the equatorial anomaly. Under the influence of a vertical  $\mathbf{E} \times \mathbf{B}$  drift the plasma associated with a particular magnetic field line is associated with a different magnetic field line at later times. Thus, in order to provide reasonable 24-hr coverage of the modeled parameters within a specified altitude and latitude region, the model equations have to be solved for many magnetic field lines.

**3.5** The continuity, momentum, and energy balance equations for each constituent ion and the electrons form a set of highly nonlinear, second-order partial parabolic equations. The equations are first linearized in them, and then finite differences are used for the spatial and temporal derivatives. The resulting coupled tri-diagonal sys-

tems of linear algebraic equations are solved by a standard technique.

**3.6** At the lower boundary of each hemisphere ( $\sim 120$  km), the ions and electrons are taken to be in chemical equilibrium, and the densities are obtained by equating the local sources and sinks. Likewise, the ion and electron temperatures are obtained by equating local heating and cooling rates.

**3.7** The time step is usually taken to be 15 min. The spatial step along the magnetic field line varies along the field line, and the number of points increases with increasing apex altitude. A mathematical formulation is used to give the point distribution. The points are arranged to give a spatial step of about 5 km at F-region altitudes.

#### 4. Model input parameters

**4.1** Latitude and longitude of ground station, day, and year.

**4.2** An IGRF (presently IGRF85) for the determination of the magnetic field.

**4.3** A solar EUV flux spectrum (presently from EUV94).

**4.4** A thermosphere model (presently MSIS86) for the determination of the neutral densities and temperatures.

**4.5** A thermospheric wind model (presently HWM90) for the determination of the meridional and zonal winds.

**4.6** A vertical  $\mathbf{E} \times \mathbf{B}$  drift model.

The model inputs described in Sec. 4.1 are read into the model from an input file. The model inputs described in Secs. 4.2–4.6 are incorporated into the model code as sets of subroutines. The subroutines permit easy modification as improved values become available and for the modifications/ changes made in applications of the model to particular studies.

#### 5. Publication references

**5.1** Bailey, G.J., and R. Sellek (1990), "A Mathematical Model of the Earth's Plasmasphere and Its Application in a Study of  $\text{He}^+$  at  $L=3.0$ ," *Ann. Geophys.* **8**, 171–190.

**5.2** Bailey, G.J., R. Sellek, and Y. Rippeth (1993), "A Modeling Study of the Equatorial Top-side Ionosphere," *Ann. Geophys.* **11**, 263–272.

#### 6. Dates of development, authors, and sponsors

##### 6.1 Dates:

1975 One-hemisphere model—ions  $\text{O}^+$  and  $\text{H}^+$ .

1978 Extended to two hemispheres.

1979  $\text{He}^+$  added to one-hemisphere model.

1980 Major revision—two-hemisphere model, axial-centered dipole magnetic field, energy balance equations, new numerical procedures for solving model equations, ions  $\text{O}^+$  and  $\text{H}^+$ .

1983  $\mathbf{E} \times \mathbf{B}$  drift added.

1990 Major revision—the ions  $\text{He}^+$ ,  $\text{N}_2^+$ ,  $\text{O}_2^+$ , and  $\text{NO}^+$  added.

1993 Major revision—magnetic field represented by an eccentric dipole.

1994 Two-stream approximation method used to determine photoelectron heating rates.

1995 Changes made to numerical procedures to improve numerical stability.

**6.2 Author (principal):** Graham J. Bailey, School of Mathematics and Statistics, Applied Mathematics Section, The University of Sheffield, Sheffield S3 7RH, UK.

**6.3 Sponsors:** Plasma Physics and Astronomy Research Council (PPARC), UK.

#### 7. Model codes and sources

The model is not user-friendly, and collaboration, in the first instance, is required between the user and the author (Graham Bailey). The author would be happy to discuss collaborations with interested groups. The author would consider enhancing/ modifying the model and model codes to meet specific requests. The model codes are written in FORTRAN and have been developed for use on a high-performance PC. It is straightforward to modify the codes for use on workstations and mainframes.

## THE FIELD LINE INTER-HEMISPHERIC PLASMA MODEL

### 1. Model content

The field line interhemispheric plasma (FLIP) model is a first-principles, one-dimensional, time-dependent chemical and physical model of the ionosphere and plasmasphere. It couples the local ionosphere to the overlying plasmasphere and conjugate ionosphere by solving the ion continuity and momentum, ion and electron energy, and photoelectron equations along entire magnetic flux tubes. The interhemispheric solutions yield densities and fluxes of  $H^+$ ,  $O^+$ ,  $He^+$ , and  $N^+$  as well as the electron and ion temperatures. In addition, continuity and momentum equations are solved to provide the densities of minor neutral species [ $N(^2D)$ ,  $N(^4S)$ ,  $NO$ ] and the first six vibrational levels of  $N_2$  in both hemispheres. A large number of other minor ion and neutral densities are calculated from chemical equilibrium between 80 and 600 km in the northern and southern hemispheres. Other outputs from the model include particle and heat fluxes, electron heating and cooling rates, photoelectron fluxes, chemical production and loss rates, and most significant airglow emission rates. Major neutral densities are supplied by the MSIS model. A three-dimensional version of the model is obtained by simulating several hundred corotating flux tubes.

### 2. Model uncertainties and limitations

**2.1** In several recent studies, the FLIP model typically produces F2 peak electron densities within 30% of the measured densities during the daytime despite the potential for large errors in several key inputs. At night, discrepancies between measured and modeled densities can often be as much as a factor of 2.

**2.2** During quiet times the error in the inputs for the solar EUV flux, MSIS neutral densities, reaction rates, and cross sections are typically about 20%. During magnetic storms uncertainties in the MSIS neutral densities may be much larger, resulting in similar errors in calculated electron densities.

**2.3** The largest uncertainty for ionospheric modeling at mid latitudes is the neutral wind magnitude. However, when measurements of  $h_mF_2$  are available, the uncertainty is reduced to about 20% by using the algorithm that we have developed.

**2.4** The current FLIP model is basically a mid-latitude model because it neglects convection electric fields, which are important at equatorial and auroral latitudes.

**2.5** The uncertainty of the plasma content of plasmaspheric flux tubes is not important during the daytime but can produce about a 50% error in calculated  $N_mF_2$  at night.

**2.6** The FLIP model is a low-speed model that is not applicable in the plasmasphere for ion densities below about  $100 \text{ cm}^{-3}$ .

### 3. Basis of the model

**3.1** The FLIP model calculates the plasma densities and temperatures along complete magnetic flux tubes from 80 km in the northern hemisphere through the plasmasphere to 80 km in the southern hemisphere as a function of time. A tilted dipole approximation is used for the Earth's magnetic field.

**3.2** The set of nonlinear, second-order, partial differential equations for continuity, momentum, and energy is transformed into finite difference equations and solved by a Newton-Raphson iterative scheme. The scheme is stable, and time steps are generally 0.5 hr except near twilight, where 10 min or less are used.

**3.3** A variable spatial grid is set up along the magnetic field line. There are approximately 200 grid points distributed in such a way as to give a grid spacing of less than 10 km in the ionosphere and less than one scale height of  $H^+$  in the plasmasphere.

**3.4** The boundary conditions imposed at the feet of the flux tube near 100 km are chemical equilibrium for ions and thermal equilibrium for temperatures. The initial plasmaspheric  $H^+$  density must also be specified.

**3.5** A unique feature of the FLIP model is the option to employ measurements of  $h_mF_2$ ,  $N_mF_2$ , and topside  $T_e$  as additional constraints for different types of studies.

### 4. Model input parameters

**4.1** The standard model can be run by simply specifying the date and the geographic location, but there are a large number of other options.

**4.2** Activity indices Kp, daily  $F_{10.7}$ , and average  $F_{10.7}$  for the MSIS neutral density, HWM93 wind, and solar EUV flux models are read from a file but can also be specified.

**4.3** Measured  $h_m F_2$ ,  $N_m F_2$ , and topside  $T_e$  can be input from a file. The  $h_m F_2$  is automatically turned into a neutral wind so that the model  $h_m F_2$  follows the observed values.

**4.4** There are a large number of adjustable parameters, such as time step and length of the run, which control the action of the model.

## 5. Publication references

**5.1** Torr, M. R., D. G. Torr, P. G. Richards, and S. P. Yung (1990), "Mid- and Low-Latitude Model of Thermospheric Emissions, 1,  $O^+(^2P)$  7320 • and  $N_2(^2P)$  3371 •," *J. Geophys. Res.* **95** (21), 147.

**5.2** Richards, P. G. (1991), "An Improved Algorithm for Determining Neutral Winds from the Height of the  $F_2$  Peak Electron Density," *J. Geophys. Res.* **96** (17), 839.

**5.3** Richards, P. G., D. G. Torr, B. W. Reinisch, R. R. Gamache, and P. J. Wilkinson (1994), "F2 Peak Electron Density at Millstone Hill and Hobart: Comparison of Theory and Measurement at Solar Maximum," *J. Geophys. Res.* **99** (15), 5.

**5.4** Richards, P. G., D. G. Torr, M. J. Buonsanto, and D. P. Sipler (1994), "Ionospheric Effects of the March 1990 Magnetic Storm: Comparison of Theory and Measurement," *J. Geophys. Res.* **99** (23), 359.

**5.5** Richards, P. G., J. A. Fennelly, and D. G. Torr (1994), "EUVAC: A Solar EUV Flux Model for Aeronomic Calculations," *J. Geophys. Res.* **99**, 8981.

**5.6** Richards, P. G., D. G. Torr, M. E. Hagan, and M. J. Buonsanto (1995), "A New Algorithm for Improved Ionospheric Electron Density Modeling," *Geophys. Res. Letters* **22**, 1385.

**5.7** Richards, P. G. (1996), "The Field Line Interhemispheric Plasma Model," *Solar-Terrestrial Energy Program: Handbook of Ionospheric Models*, edited by R.W. Schunk, p. 207.

## 6. Dates of development, authors, and sponsors

### 6.1 Dates:

1979 Development of interhemispheric solutions for  $[O^+]$ ,  $[H^+]$ ,  $T_e$ , and  $T_i$ .

1980 Interhemispheric solutions for photoelectron flux and solutions for minor ion and neutral densities added.

1981 Diffusion equations for vibrationally excited  $N_2$  effects included.

1982 Improvements to the photoelectron flux model to reproduce observed flux.

1986 Developed original algorithm for obtaining winds from  $h_m F_2$ .

1991 Improved algorithm for getting winds from  $h_m F_2$ .

1992 Added energetic electron precipitation for auroral studies.

1993 Developed algorithm to cause model to reproduce both  $h_m F_2$  and  $N_m F_2$ .

1994 Developed EUVAC solar EUV flux model.

1995 Developed algorithm to reproduce observed topside ionosphere.

**6.2 Author (principal):** Phil Richards, Computer Science Department, The University of Alabama in Huntsville, Huntsville, AL 35899, USA.

**6.3 Sponsors:** National Aeronautics and Space Agency, National Science Foundation.

## 7. Model codes and sources

A VAX version of the model is available to be installed at the user's institution. A UNIX version is also under development. The model runs from DEC command files that are well documented. There is also an interface that helps the user understand the model and aids in the setting up of the DEC command files. Some previous users with a good knowledge of the ionosphere have been able to run the model with little additional help. The author also runs the model for collaborative studies. Contact person: Phil Richards, Computer Science Department, The University of Alabama in Huntsville, Huntsville, AL 35899, USA (e-mail richards@cs.uah.edu).

## ALGEBRAIC MODEL

### 1. Model content

The D region has the most complex chemistry of any ionospheric region by far, and, to this day, its chemistry has not been elucidated fully. Nevertheless, there has been success in modeling the D region, especially the electron concentrations of the disturbed D region. This achievement has been made possible largely because ion-ion recombination (neutralization) coefficients all appear to be near  $10^{-7} \text{ cm}^{-3} \text{ s}^{-1}$  (Smith et al., 1976) regardless of the type of ions involved. Hence, even though the negative ion chemistry is still unsatisfactory as to the concentrations of the various individual ions, the electron concentration can be determined with some confidence, as seen in Fig. 1 of Smith (1976), where the model to be discussed is shown to match well the upleg data for a Solar Proton Event (SPE) or Polar Cap Absorption (PCA) event.

The formation of the model is purely a sequence of algebraic expressions that yield solutions, after sufficient iterations, for the electron concentration [e] and all the individual ions currently in the model: 21 positive ions and 8 negative ions. Especially for disturbed events, but even for quiet conditions, D-region processes are sufficiently rapid, compared with the complexity of the chemistry, that steady-state conditions are appropriate, except during twilight.

Transport is ignored. Collision frequencies may be included for calculating the absorption of electromagnetic waves (Swider and Chidsey, 1977).

### 2. Model uncertainties and limitations

The model has been fitted well to the November 1969 PCA event (Swider and Foley, 1978; Swider, 1988). Indeed, for electron concentrations under disturbed condition, the day and night empirical expressions given above for initial [e] may be sufficiently accurate (Swider, 1988). For quiet conditions, the accuracy of the outputs is less certain, in part because D-region data for quiet conditions are also of low accuracy.

### 3. Basis of model

An iterative scheme was developed to solve for all species concentrations. Using initial concentrations for electrons [e] and the positive ion sum SP, the individual negative ion concentrations are

first determined and summed, NSUM. Then the positive ions are individually calculated and summed, PSUM. A new

$$[e] = \{\text{previous } [e] + \text{PSUM}/(1+\lambda)\}/2 \quad (1)$$

where  $\lambda = \text{NSUM}/\text{previous } [e]$ , and a new

$$\text{SP} = \{\text{previous } [e] + \text{NSUM} + \text{PSUM}\}/2 \quad (2)$$

are then determined. This sequence is repeated until  $\text{PSUM} = \text{NSUM} + [e]$  within a specified precision. For the November 1969 SPE, not more than nine iterations were required to reach  $\pm 1\%$  for altitudes 40–90 km.

Initial daytime concentrations were derived from  $[e] - (q/\Psi)^{-}$ , where the effective recombination coefficient  $\Psi$  is that derived from the Nov. 2–5, 1969, SPE (Swider and Dean, 1975). The values determined (in  $\text{cm}^{-3} \text{ s}^{-1}$ ) were  $3.4 \times 10^{-7}$  (85 km),  $4.8 \times 10^{-7}$  (80 km),  $1.1 \times 10^{-6}$  (75 km),  $1.8 \times 10^{-6}$  (70 km),  $4 \times 10^{-6}$  (65 km),  $8.8 \times 10^{-6}$  (60 km),  $5.5 \times 10^{-5}$  (55 km),  $5.1 \times 10^{-4}$  (50 km), and  $3.5 \times 10^{-2}$  (45 km).

Initial nighttime electron concentrations were derived from (Swider et al., 1975)

$$[e] = \{(L(A)/2\alpha_D)^2 + q/\alpha_D\}^{-} - L(A)/2\alpha_D \quad (3)$$

where the mean (ion-electron) recombination coefficient  $\alpha_D$  is  $4 \times 10^{-7} \text{ cm}^{-3} \text{ s}^{-1}$ , and where

$$L(A) = k_{61}\{\text{O}_2\}^2 + k_{62}[\text{O}_2][\text{N}_2] \quad (4)$$

is the loss rate ( $\text{s}^{-1}$ ) for electrons through attachment to  $\text{O}_2$ , with  $k_{xx}$  a specific reaction rate.

Initial total positive ion concentrations were determined from

$$\text{SP} = \{q(5[\text{O}]/\alpha_D + [\text{O}_3]/\alpha_i)/(5[\text{O}] + [\text{O}_3])\}^{-} \quad (5)$$

with  $\alpha_i$  the mean ion-ion recombination coefficient,  $6 \times 10^{-8} \text{ cm}^{-3} \text{ s}^{-1}$ .

Concentrations of electrons, 21 positive ions and 8 negative ions, are determined to two significant figures. Also printed are  $q$ ,  $\lambda$ ,  $\Psi$ ,  $L(A)$ ,  $\text{PSUM}$ ,  $\text{NSUM} + [e]$ , initial [e], and initial SP.

### 4. Model input parameters

The following neutral concentrations are required: O, O<sub>2</sub>, O<sub>3</sub>, O<sub>2</sub>(<sup>1</sup>Δ), N<sub>2</sub>, CO<sub>2</sub>, H<sub>2</sub>O, NO, NO<sub>2</sub>, temperature T, and total neutral concentration M. The relationships [N<sub>2</sub>] = 0.7808[M], [O<sub>2</sub>] = 0.2095[M], CO<sub>2</sub> = 3 × 10<sup>-4</sup>[M] may be used. Values for total ionization production q must be provided. For quiet conditions in the daytime, q may be derived from the photoionization of NO by H Lyα, nominally (Swider, 1978)

$$q(\text{NO}^+) = 6 \times 10^{-7} [\text{NO}] \exp\{-10^{-20} [\text{O}_2] H\} \quad (6)$$

where H is the scale height of the atmosphere.

Processes and rate coefficients are listed in Tables 1 and 2 of Swider (1978). Photodissociation rates were multiplied by unity for daytime and zero for nighttime. Choices for α<sub>i</sub> and α<sub>D</sub> were given above.

## 5. Publication references

**5.1** Smith, D., N.G. Adams, and M.J. Church (1976), *Planetary Space Sci.* **24**, 697–703.

**5.2** Swider, W. (1978), *J. Geophys. Res.* **83**, 4407–4410.

**5.3** Swider, W. (1988), *PAGEOPH* **127**, 403–414.

**5.4** Swider, W., and I.L. Chidsey Jr. (1977), *J. Geophys. Res.* **82**, 1617–1619.

**5.5** Swider, W., and W.A. Dean (1975), *J. Geophys. Res.* **80**, 1815–1819.

**5.6** Swider, W., and C.I. Foley (1978), AFGL-TR-78-0155.

**5.7** Swider, W., R.S. Narcisi, T.J. Keneshea, and J.C. Ulwick (1971), *J. Geophys. Res.* **76**, 4691–4694.

## 6. Model codes and sources

The model (Swider and Foley, 1978) may be ordered from National Technical Information Service.

## NUMERICAL MODEL OF D-REGION ION CHEMISTRY, 1995

### 1. Model content

The numerical model Sodankyla Ion Chemistry (SIC) was developed as an alternative approach to those D-region ion-chemistry models that combine the more doubtful chemical reactions to effective parameters, the values of which are set against experimental data. A detailed chemical scheme, in a conceptually simple model, was built to be a tool for interpretation of D-region incoherent scatter experiments and cosmic radio-noise absorption measurements, both of which form the basis of D-region research done at Sodankyla Geophysical Observatory. The number of different ions in the current version is 55, of which 36 are positive and 19 are negative. The model was first applied by Burns et al. (1991) in a study of incoherent scatter measurements. A detailed description of the first version of the model is given by Turunen et al. (1992, 1996). The SIC model can be run either as a steady-state model or a time-dependent model. The model solves for ion and electron concentrations in ionospheric D and lower E regions. Local chemical equilibrium can be calculated in the altitude range from 50 to 100 km at 1-km steps. The solution for the steady state can be advanced in time to solve for response of the ion concentrations to a sudden disturbance, e.g., in ion production rates or in neutral-gas properties. Originally the model was developed for applications during geophysically quiet conditions. Consequently, as ionization sources acting on five primary neutral components  $N_2$ ,  $O_2$ ,  $O$ ,  $NO$ , and  $O_2(^1\Delta_g)$ , the solar radiation at wavelength range 5–134 nm and galactic cosmic rays were considered. At present, however, the model is extended to include electron precipitation as an ionization source. A similar extension was made to use the model during solar-proton events, as in the application of the SIC model by Turunen (1993).

### 2. Model uncertainties and limitations

A detailed ion-chemical scheme with many reactions is subject to the uncertainties and inaccuracies in the reaction rate constants. Neutral chemistry and ion chemistry are not coupled in this model. The neutral atmosphere is taken only as a static background. If the effect of particle fluxes is considered in detail, one should care about the dissociation of neutral minor constituents. For investigations around sunset and sunrise, the ef-

fects of neutral photochemistry should be included in detail. Hard x rays and scattered radiation at night are not included as ionization sources. In addition to the presently included components, heavier cluster ions, heavier clusters of negative ions, and more metallic ions are known to exist in the D region. The assumptions on which the model is based are as follows:

- 1) The neutral atmosphere is described by the semi-empirical model MSIS-90 (Hedin, 1991).
- 2) The ionospheric D region is sunlit. This restricts the range of the solar zenith angle to be below 95 deg.
- 3) Ionization during quiet time is primarily caused by photoionization and galactic cosmic rays. Ionization by solar protons and precipitating electrons is calculated using measured particle-energy deposition rates in air.
- 4) We neglect any transport effects. Chemical lifetimes of the ions are assumed to be short with respect to transport processes.
- 5) The concentrations of neutral species are much higher than those of ions and thus assumed to be unaffected by ion chemistry.
- 6) An overall charge neutrality prevails.

### 3. Basis of the model

In addition to the above-mentioned neutrals, Ar, He, and  $CO_2$  also are included in photoionization calculations, because they absorb the solar radiation at the relevant wavelength range. To account for important ion-chemical reactions we need to include also  $H_2O$ ,  $N$ ,  $H$ ,  $O_3$ ,  $OH$ ,  $NO_2$ ,  $HO_2$ ,  $NO_3$ ,  $HNO_2$ ,  $CO_3$ ,  $H_2$ ,  $HCl$ ,  $HNO_3$ ,  $Cl$ ,  $ClO$ ,  $CH_4$ , and  $CH_3$  in the list of the neutral components of the model.

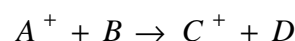
Continuity equation for ion  $i$  (transport effects neglected):

$$\frac{dn_i}{dt} = P_i - n_i \cdot L_i$$

where

$$P_i = \sum_{\text{production}} p_{im} \quad , \quad L_i = \sum_{\text{loss}} l_{im} \quad m$$

Consider reaction



for

$$C^+ :$$

and for

$$A^+ : l_{A^+m} = k[A^+][B]$$

Assume constant neutral concentrations:

$$p_{C^+m} = \Pi_{C^+m}[A^+], l_{A^+m} = \Lambda_{A^+m}[A^+]$$

Continuity equation in matrix form:

$$\frac{d\hat{N}}{dt} = \vec{F}(\vec{N}) = \Gamma(\vec{N})\vec{N} + \vec{Q}(\vec{N})$$

$\Gamma$  is a  $55 \times 55$  matrix. Elements  $\Pi$  and  $\Lambda$  describe the production and loss rates of each ion.  $\hat{N}$  is a vector containing the 55 unknown ion concentrations.  $\vec{Q}$  is a vector that contains the constant primary ionization rates. Chemical equilibrium may be solved by setting

$$\frac{dn_i}{dt} = 0$$

Starting from the equilibrium solution of the ion concentrations, we advance the concentrations in time by taking small time steps according to the expression

$$\vec{N}_{n+1} = \vec{N}_n + \Delta t \left[ \vec{F}(\vec{N}_n) + \frac{d\vec{F}}{d\vec{N}} \Big|_{\vec{N}=\vec{N}_n} \cdot (\vec{N}_{n+1} - \vec{N}_n) \right]$$

where the elements  $f_{ij}$  of the matrix

$$\frac{d\vec{F}}{d\vec{N}} \Big|_{\vec{N}=\vec{N}_n}$$

are the partial derivatives

$$f_{ij} = \frac{dF_i}{dN_j} \Big|_{\vec{N}=\vec{N}_n}$$

The expression above is a set of linear equations,

which has to be solved for each time step.

#### 4. Database and input to the model

As input to the neutral atmosphere model, MSIS-90, one gives time, location, and information about solar and geomagnetic activity. The resulting neutral constituent concentrations are then used to calculate ion production rates and chemical reaction rates. For those neutral constituents that are not covered by the MSIS-90 model, fixed reference profiles may be selected. Also fixed mixing ratios of  $3 \times 10^4$  and  $1 \times 10^6$  for  $\text{CO}_2$  and  $\text{H}_2\text{O}$ , respectively, can be used. Some applications may require that a set of the neutral minor constituent profiles is kept fixed while selected concentrations are varied.

Absorption cross sections for  $\text{N}_2$ ,  $\text{O}_2$ ,  $\text{O}$ , and  $\text{He}$  are from Torr et al. (1979); for  $\text{NO}$  and  $\text{Ar}$ , the constants from the tables of Ohshio et al. (1966) are used; and for  $\text{CO}_2$ , the data are from McEwan and Phillips (1975). Photoionization efficiencies come from the same references as the absorption cross sections.

A reference solar spectrum was collected from the spectrum by Torr et al. (1979) and from spectrum R74113 by Heroux and Hinteregger (1978). The intensities for wavelengths 103.76 nm and 110.8 nm were taken from the paper of Huffman et al. (1971). For our reference spectrum, Ly- $\alpha$  line was chosen from Lean and Skumanich (1983). The intensities can be varied according to the chosen level of solar activity. Heaps (1978) has derived a convenient parametrization of the empirical rate of ion-pair production by cosmic rays,  $Q_{\text{cr}}$ , as a function of latitude, altitude, and solar activity.

The spectrum of precipitating electrons can be given in a parameterized form of the differential energy spectrum. Alternatively, a precise form of the spectrum can be given, e.g., in the form of fluxes at selected energy channels. Input of the proton flux is formulated to correspond to measurements at predefined energy channels, as, e.g., those used by the satellite GOES-7.

For the chemical schemes, the main contributions were taken from the works by Chakrabarty et al. (1978), Dymek (1980), Wisenberg and Kockarts (1980), Torkar and Friedrich (1983), and Thomas and Bowman (1985). The reaction rate constants were updated from several sources.

## 5. Publication references

**5.1** Burns, C.J., E. Turunen, and H. Matveinen (1991), *J. Atmos. Terr. Phys.* **53**, 115.

**5.2** Chakrabarty, D.K., P. Chakrabarty, and G. Witt (1978), *J. Atmos. Terr. Phys.* **40**, 437.

**5.3** Dymek M.K. (1980), *Low Latitude Aeronomical Processes*, edited by A.P. Mitra, COSPAR Symposium Series, Pergamon Press, Oxford and New York, Vol. 8, p. 118.

**5.4** Heaps, M.G. (1978), *Planetary Space Sci.* **26**, 513.

**5.5** Hedin A.E. (1991), *J. Geophys. Res.* **96**, 1159.

**5.6** Heroux, L., and H.E. Hinteregger (1978), *J. Geophys. Res.* **83**, 5305.

**5.7** Huffman, R.E., D.E. Paulsen, and J.C. Larrabee (1971), *J. Geophys. Res.* **76**, 1028.

**5.8** Lean, J.L., and A. Shumanich (1983), *J. Geophys. Res.* **88**, 5751.

**5.9** McEwan, M.J., and L.F. Phillips (1975), *Chemistry of the Atmosphere*, Edward Arnold Ltd., London.

**5.10** Ohshio, M., R. Maeda, and H. Sakagami (1966), *J. Radio Res. Lab.* **13**, 245.

**5.11** Thomas, L., and M.R. Bowman (1985), *J. Atmos. Terr. Phys.* **47**, 547.

**5.12** Torkar, K.M., and M. Friedrich (1983), *J. Atmos. Terr. Phys.* **45**, 369.

**5.13** Torr, M.R., D.G. Torr, R.A. Ong, and H.E. Hinteregger (1979), *Geophys. Res. Letters* **6**, 771.

**5.14** Turunen E. (1993), *J. Atmos. Terr. Phys.* **55**, 767–781.

**5.15** Turunen, E., H. Matveinen, and H. Ranta (1992), "Sodankyla Ion Chemistry (SIC) Model," Sodankyla Geophysical Observatory, Rept. 49,

Sodankyla, Finland.

**5.16** Turunen, E., J. Tolvanen, H. Matveinen, and H. Ranta (1996), "D Region Ion Chemistry Model," *STEP Handbook of Ionospheric Models*, edited by R.W. Schunk.

**5.17** Wisenberg, J., and G. Kockarts (1980), *J. Geophys. Res.* **85**, 4642.

## 6. Dates of development, authors, and sponsors

### 6.1 Dates:

1989 Version 1.0, 35 ions.

1991 Version 1.1, reaction rates updated.

1994 Version 2.0, adding and removing reactions.

1995 Version 2.1, 55 ions.

1995 Version 3.0, time-dependent code.

**6.2 Author (principal):** Esa Turunen, Head of the Ionospheric Station, SGO; Helena Matveinen, Scientist, SGO.

**6.3 Sponsor:** Finnish Academy of Science and Letters, Geophysical Observatory, Sodankyla, Finland.

## 7. Model codes and sources

The early versions of the model were based on FORTRAN code, which we no longer support. The present version of the model is coded in MATLAB language, which makes the model user-friendly, easy to adapt, and easy to tailor to specific needs. The current version is written using MATLAB 4.2c. The code runs on computers that can run MATLAB. The code is not optimized for speed, but this could be done by any user. The latest version will be made available to anyone interested. Contact person: Esa Turunen, Sodankyla Geophysical Observatory, FIN-99600 Sodankyla, Finland (e-mail: Esa.Turunen@sgo.fi).

## SOLAR EUV AND CHEMISTRY MODEL

### 1. Model content

A modeling technique of Keneshea (1967) was applied by Keneshea et al. (1970) to the E region for detailed comparisons with ionic compositions measured at twilight (two at sunset and two at sunrise). The experiments were conducted under normal (quiet) conditions at mid latitudes, near Eglin Air Force Base, Florida, during April 1967. This month was one of moderate solar activity, with a mean sunspot number of 69.5.

### 2. Model uncertainties and limitations

It is our experience that [NO] appears generally to be greater in the E region than many models assume. Thus some models yield  $O_2^+ \gg NO^+$  near 95–100 km, whereas the observational data, with perhaps one exception, do not support this result (Swider, 1994). The values of [NO] used here are in the higher range of those determined from gamma-band data. However, these values have worked well. Again, our use of a somewhat higher x-ray flux appears justified by the model's favorable comparison with the observational ionic data. There have been suggestions that there is insufficient ionization produced near 95–100 km, implying a missing source of ionization. However, none have offered any specific details, and our model agrees quite well with incoherent scatter data in the lower E region (Trost, 1979).

### 3. Basis of model

The model was set up to simultaneously solve a set of coupled partial differential equations

$$\frac{dn_i}{dt} = Q_i - L_i \quad (1)$$

where  $n_i$  is the number density of the  $i$  species, with  $Q_i$  and  $L_i$  the respective production and loss terms for that species, which terms commonly include other species concentrations.

Concentrations were calculated for negative ions  $O^-$ ,  $O_2^-$ ,  $O_3^-$ ,  $NO_2^-$ ,  $NO_3^-$ , and  $CO_3^-$ ; positive ions  $O^+$ ,  $O_2^+$ ,  $N_2^+$ , and  $NO^+$ ; and electrons  $e$ . In addition, differential equations were solved for the following neutral species: NO, N,  $NO_2$ , O,  $N_2O$ ,  $O_3$ ,  $CO_2$ ,  $H_2$ , H, OH,  $HO_2$ ,  $H_2O$ ,  $H_2O_2$ ,  $O_2$ , and  $N_2$ . However, in applying the code to the E region, NO and N were held fixed. The major gases changed very little over the course of the run: about one day commencing at noon, when the

solar zenith angle was 21.6 deg. The major species ( $O_2$ ,  $N_2$ ) changed imperceptibly over this period, and negative ions were negligible. As we were not focusing on the chemistry of the minor neutrals but rather on the major positive ions and electrons, we list only their relevant chemistry (Summary of Reference and Standard Ionospheres), which has changed little over the intervening years.

Transport was ignored in this model. However, because one sunset observation was quite distorted, a special calculation was performed (Keneshea and MacLeod, 1970), which compared well with the data. This model variation included transport terms using the full continuity equations. The velocities required for the divergence term were derived from the measured neutral wind profiles for an earlier flight and used in a collision-geomagnetic equilibrium expression

$$v_i = \frac{1}{1 + r_i^2} [r_i^2 u + r_i u \times \Gamma + (u \cdot \Gamma) \Gamma], \quad (2)$$

where  $p_i$  is the ratio of neutral-ion collision frequency to gyrofrequency,  $\Gamma$  a unit vector in the geomagnetic field direction, and  $u$  the neutral wind (MacLeod, 1966).

The method of solution for the partial differential equations uses a fourth-order Runge Kutta integration with a variable mesh. When a species enters its quasi-equilibrium state, its differential equation is removed from the set, and its equilibrium equation is inserted into the simultaneous algebraic set, which is solved by the methods of successive substitutions. The overall solution is obtained by iteration between the differential and algebraic sets.

A numerical solution to this problem that requires the use of a high-speed digital computer has been discussed (Keneshea, 1962). The computer program resulting from that study, although it developed satisfactory solutions within a minimum of computer time, can be used only at E-region altitudes. One reason for this restriction is that the number density of  $NO^+$  ions is always computed from the requirement of balance of charge. (The sum of the positive ions equals the sum of the electrons and the negative ions.) This method is applicable, however, only if  $NO^+$  is the most abundant ion. Although this appears to be true in the E region, it will not be the case at lower altitudes, in the D region. Because the system is solved on a digital computer, it is not possible to

accurately determine the concentration of a minor species through conservation of charge. The required number density is located in the least significant bits of the computer word, and, depending upon the amount of accumulated round-off error, the result could be erroneous.

#### 4. Model input parameters

Solar fluxes and absorption cross sections were taken from Watanabe and Hinteregger (1962) above about 100Å. Below this wavelength, the values listed by Nicolet and Aiken (1960) for quiet solar conditions were adopted. The solar flux in the range 10–170Å was increased by a factor of 4 over the values cited above in order to best match the data. The proper x-ray flux for the E region is still of concern in more recent codes which aim to determine minor odd nitrogen species, particularly N and NO. An H Ly $\alpha$  flux of 4 egs cm<sup>-2</sup> sec<sup>-1</sup> was adopted, and the ionization effects of the scattered H Ly $\alpha$  and H Ly $\beta$  radiations were approximated by setting their fluxes at 1% and 0.4%, respectively, of their noontime height-dependent direct flux profiles. The paper by Strobel et al. (1980) should be consulted for a detailed analysis of nighttime ionization sources and their intensities. The declination of the sun was fixed at 8.62 deg for comparison with the specific experimental data, with the noontime solar zenith angle  $\chi$  being 21.63 deg. Atmospheric concentrations and temperatures were taken from the mean 1965 COSPAR International Reference Atmosphere (CIRA). All particles were assumed to have the same temperature distribution. In calculating the optical depth, appropriate CIRA concentrations were integrated along the various solar zenith angles. The nitric oxide concentrations essentially were a smooth version of Barth's (1966) results, but lower at 85 km, the lowest altitude of the calculation. Atomic nitrogen concentrations were effectively negligible,  $[N] = 10^{-2}[NO]$ . Both species were held constant throughout the time-dependent solutions of the charged constituents.

The specific nitric oxide concentrations used were (in 10<sup>6</sup> cm<sup>-3</sup>) 3 (140 km), 5.4 (130 km), 11 (120 km), 25 (110 km), 34 (105 km), 40 (100 km), 38 (95 km), 25 (90 km), and 10 (85 km). Calculations were performed only at these altitudes. Nitric oxide plays two major roles. First, it converts O<sub>2</sub><sup>+</sup> ions into NO<sup>+</sup> ions via the charge transfer reaction (#9 in Summary of Reference and Standard Ionospheres). However, it is the product  $k_9 [NO]$  that is

important. Thus, as  $k_9$  is now about 25% lower than the value in Summary of Reference and Standard Ionospheres, the  $[NO]$  used is effectively 4/3 the values cited. More significant is that, near a solar zenith angle of 90 deg, the attenuation of H Ly $\alpha$  near 100–110 km is negligible, and the main ionization source is therefore H Ly $\alpha$  + NO  $\rightarrow$  NO<sup>+</sup> + e. If  $[NO]$  is enhanced, as is often the case for the auroral region (discussed below), E-region concentrations  $[e]$  at sunrise increase, too, as  $[e]^2$  is proportional (numerically) to  $[NO]$  (Swider and Keneshea, 1993).

#### 5. Publications references

- 5.1 Barth, C.A. (1966), *Ann. Geophys.* **22**, 198–207.
- 5.2 Keneshea, T.J. (1967), AFCRL-67-0221.
- 5.3 Keneshea, T.J., and M.A. MacLeod (1970), *J. Atmos. Sci.* **27**, 981–984.
- 5.4 Keneshea, T.J., R.S. Narcisi, and W. Swider Jr. (1970), *J. Geophys. Res.* **75**, 845–854.
- 5.5 Nicolet, M., and A.C. Aikin (1960), *J. Geophys. Res.* **65**, 1469–1483.
- 5.6 Stobel, D.F., C.B. Opal, and R.R. Meier (1980), *Planetary Space Sci.* **28**, 1027–1033.
- 5.7 Swider, W., and T.J. Keneshea (1993), *J. Geophys. Res.* **98**, 1725–1728.
- 5.8 Swider, W. (1994), *EOS* **75**, 246.
- 5.9 Trost, T.F. (1979), *J. Geophys. Res.* **84**, 2736–2742.
- 5.10 Watanabe, K., and H.E. Hinteregger (1962), *J. Geophys. Res.* **67**, 999–1006.

#### 6. Model codes and sources

A version of the model may be available (contact W. Swider), but it may not be worth running in view of the published outputs, especially because others undoubtedly have codes much faster than the one discussed here. The original printout is available (W. Swider). The originator/writer of the code (T.J. Keneshea) has expanded it to include transport and IR emissions, but its availability through Visidyne Research, Inc., may be limited.

## AFRL BOLTZMANN-FOKKER-PLANCK MODEL FOR THE DAYTIME LOWER IONOSPHERE

### 1. Model content

The Boltzmann-Fokker-Planck (BFP) model calculates the energy-dependent electron distribution function, the electron density, the electron temperature, and the densities of four ion species ( $O^+$ ,  $N_2^+$ ,  $O_2^+$ ,  $N_2^+$ ) in the earth's daytime lower ionosphere. Electron and ion production rates per unit volume are also calculated. The model assumes a steady state and uses a local approximation. Thus the above quantities are calculated for a given time, location, and altitude. To develop any spatial or temporal information requires that a series of calculations be made for the different altitudes, locations, and times of interest. Past use has usually focused on several altitudes at a specific time and place.

### 2. Model uncertainties and limitations

One source of model inaccuracy lies in the uncertainties in our knowledge of various cross sections and reaction rates needed for the calculation. Fortunately, most of the cross sections and reaction rates have been measured so that there is an empirical basis for the values that are used. Another limitation to the model accuracy occurs because of the need to know the geophysical conditions of the time and place being modeled.

As described earlier, the model is restricted to the lower ionosphere, which typically means the E and F1 regions. In previous work, the model has been used down to around 100 km. There is potential for going down to around 90 km. However, in any particular case, the appropriate lower boundary is defined wherever processes normally associated with the D region can no longer be neglected. The upper boundary is typically slightly below the F2 peak and, for any particular case, should be determined by where electron and ion transport become important. At mid latitudes this altitude is typically 220–250 km.

The model is strictly a daytime model, with the solar flux acting as the primary source of ionization. As such, it is generally inappropriate for use in the auroral regions or any daytime location that is undergoing significant particle precipitation.

The model calculates the zero-order state of the photoelectron distribution function and does not

include any wave-particle or wave-wave plasma interactions.

### 3. Basis of the model

The BFP model produces a numerical solution of a kinetic equation for the isotropic portion of the steady-state electron distribution function (EDF) and of four ion continuity equations for the ion densities. The equations solved can be derived by beginning with a system of one-particle plasma kinetic equations, where one equation appears for each state of each kind of particle. By assuming that the ion distribution functions are local Maxwellian functions and that transport effects can be neglected (local approximation), a steady-state equation for each ion density can be derived. For the lower ionosphere, this results in four coupled equations for the ion densities. In these four equations, there are terms that depend on the energy-dependent EDF, which is considered unknown. An equation for this distribution function is derived by assuming a steady state, by neglecting the anisotropic portion of the distribution function, and by integrating the kinetic equation for the EDF over angles in velocity space. The resulting equation contains a series of terms that describe the rates of change of the EDF due to photoionization and collision processes. The name of the model comes from the fact that the explicit expressions for each of these terms come from using either Boltzmann or Fokker-Planck methods. Finally, both the electron density and temperature can be found from their definitions once the EDF is known. The primary sources and sinks of ionization are photoionization and recombination, respectively. The electron-neutral processes included are elastic collisions, excitation collisions, de-excitation collisions, and ionizing collisions. Also included are elastic electron-ion and electron-electron collisions. These terms are nonlinear in the EDF and are formulated in terms of the Rosenbluth potentials. Included are a variety of chemical reactions that involve the above ions and the three major neutral species ( $O$ ,  $N_2$ ,  $O_2$ ) of the earth's atmosphere.

In solving the kinetic equation for the EDF, a nonuniform grid of several hundred energy points is used that typically spans from  $1 \times 10^{-9}$  to 225 eV. As mentioned, a single computer run of the model performs the calculation for a specific altitude, time, and location.

### 4. Model input parameters

The model requires geophysical inputs as well as a variety of cross sections and reaction rates. The cross sections and rates are provided by a series of data files that can be updated whenever new values are available. The geophysical inputs are the solar flux, neutral densities, neutral temperatures, and ion temperatures. These are generally supplied by empirical or statistical models for these quantities.

## 5. Publication references

**5.1** Jasperse, J.R. (1976), "Boltzmann-Fokker-Planck Model for the Electron Distribution Function in the Earth's Ionosphere," *Planetary Space Sci.* **24**, 33–40.

**5.2** Jasperse, J.R. (1977), "Electron Distribution Function and Ion Concentrations in the Earth's Lower Ionosphere from Boltzmann-Fokker-Planck Theory," *Planetary Space Sci.* **25**, 743–756.

**5.3** Jasperse, J.R. (1981), "The Photoelectron Distribution Function in the Terrestrial Ionosphere," *Physics of Space Plasmas*, edited by T. Chang, B. Coppi, and J. R. Jasperse, SPI Conference Proceedings and Reprint Series, Scientific Publishers, Cambridge, MA, Vol. 4, p. 53.

**5.4** Winningham, J.D., D.T. Decker, J.U. Kozyra, J.R. Jasperse, and A.F. Nagy (1989), "Energetic (> 60 eV) Atmospheric Photoelectrons," *J. Geophys. Res.* **94**, 15,335–15,348.

## 6. Dates of development, authors, and sponsors

### 6.1 Dates:

1973 Coupled nonlinear equations for electron distribution function in the earth's ionosphere are derived.

1976 Numerical solution of electron kinetic equation and local ion continuity equations is completed.

1982 Low-energy electron and photon cross sections are updated.

1989 BFP model compared with other photoelectron models.

**6.2 Authors:** John R. Jasperse, Phillips Laboratory/GPIM; Neil J. Grossbard, Boston College; and Dwight T. Decker, Boston College.

**6.3 Sponsors:** Air Force Office of Scientific Research and Phillips Laboratory of the U. S. Air Force Material Command.

## 7. Model codes and sources

The model is in the form of a large FORTRAN code, but it is not user friendly. Anyone interested in results from this code should contact John R. Jasperse.

## AFRL TRANSPORT MODEL FOR THE ELECTRON-PROTON-HYDROGEN ATOM AURORA

### 1. Model content

The PL transport model for the combined electron-proton-hydrogen atom aurora describes the energy deposition, ionization, and excitation of optical emissions by the precipitating electrons, protons, and hydrogen atoms associated with the auroral zone for steady-state conditions. The numerical code solves a coupled set of three linear transport equations for the three particle species to obtain the particle fluxes as functions of altitude, energy, and pitch angle. The altitude profiles of the rates of energy deposition, ionization, and excitation of optical emissions are then calculated from the fluxes. The code also calculates the electron-density profile associated with the combined aurora. Densities of the important ion species are calculated by using a detailed chemistry model that solves a set of coupled rate equations. The electron density is then specified by requiring charge neutrality. The model can also be used to study a pure electron aurora or a pure proton-hydrogen-atom aurora by choosing the appropriate boundary conditions. At present the model calculates volume emission rates for the following optical features:  $N_2^+$  first negative group (3914 Å),  $N_2$  second positive group (3371 Å), selected  $N_2$  Lyman-Birge-Hopfield bands (1325 Å, 1354 Å, 1383 Å, 1493 Å, and all bands between 1700 and 1800 Å), OI (1356 Å), NI (1493 Å),  $L\alpha$  (1216 Å), H $\beta$  (4861 Å), and H $\alpha$  (6563 Å). More optical features will be added to the model as their cross sections become available.

The transport model assumes steady-state conditions with no electric fields present, plane-parallel geometry, and a uniform geomagnetic field (magnetic mirroring effects are neglected). The effect of the atmospheric lateral spreading of the incident proton stream due to charge-changing processes (charge exchange and stripping), which is neglected in the plane-parallel geometry, can be included, to a good approximation, by multiplying the incident flux with an appropriate correction factor (Jasperse and Basu, 1982).

The inputs for the model are (1) the cross sections for the various collision processes involving electrons, protons, and hydrogen atoms; (2) effective cross sections for selected emission features; (3) the neutral atmosphere; and (4) the in-

cident particle (electron and proton) fluxes at the upper boundary of the atmosphere.

### 2. Model uncertainties and limitations

**2.1** The reliability of the calculated aurora-related quantities largely depends on the accuracy with which the input quantities can be specified.

**2.2** The steep bottomside profile, which is the general characteristic of the precipitating particle fluxes, requires fine altitude grid points to obtain a desired accuracy.

**2.3** The model does not take into account the effect of magnetic mirroring on the pitch-angle distribution of the particle fluxes.

### 3. Basis of the model

The model is based on a coupled set of three transport equations for the electrons, protons, and hydrogen (H) atoms that includes all the elastic and inelastic collision processes involving these particles and the neutral particles. The proton and H atom fluxes are coupled only to each other because of the charge-changing collisions, whereas the electron flux is coupled to both the proton and the H atom fluxes through the secondary electrons that they generate. The equations for protons and H atom fluxes are first converted into integral equations and then solved on a two-dimensional grid of energy (E) points from  $E_{\min}$  to  $E_{\max}$  and altitude (z) points from  $z_{\min}$  to  $z_{\max}$  (for details, see Basu et al., 1990). These fluxes are used to calculate the secondary-electron source terms in the electron transport equation. The electron transport equation is then solved to obtain the degraded primary and secondary electron fluxes by using a discrete ordinate and eigenvalue technique (for details, see Strickland et al., 1976; Basu et al., 1993). From the particle fluxes as a function of altitude, energy, and pitch angle, various quantities of interest are calculated by using rigorous theoretical formulae (Basu et al., 1993).

### 4. Model input parameters

**4.1** The set of particle impact and effective emission cross sections used in the model and the sources of these cross sections are given by Basu et al. (1990) and Strickland et al. (1993).

**4.2** The model can use any neutral atmosphere specified by the user. Presently, it uses the MSIS-86 thermospheric model.

**4.3** The incident electron and proton fluxes are specified by analytic functions. Two commonly used energy distributions for the incident electron flux are (1) a Maxwellian distribution with the options of adding low- and high-energy tails and (2) a Gaussian distribution with the same options. For the protons, a Maxwellian or a Kappa distribution, or some combination of them, is used.

## 5. Publication references

**5.1** Basu, B., J.R. Jasperse, and N.J. Grossbard (1990), "A Numerical Solution of the Coupled Proton-H Atom Transport Equations for the Proton Aurora," *J. Geophys. Res.* **95**, 19,069.

**5.2** Basu, B., J.R. Jasperse, R.M. Robinson, R.R. Vondrak, and D.S. Evans (1987), "Linear Transport Theory of Auroral Proton Precipitation: A Comparison with Observations," *J. Geophys. Res.* **92**, 5920.

**5.3** Basu, B., J.R. Jasperse, D.J. Strickland and R.E. Daniell (1993), "Transport-Theoretic Model for the Electron-Proton-Hydrogen Atom Aurora, 1. Theory," *J. Geophys. Res.* **98**, 21,517.

**5.4** Daniell, R.E., and D.J. Strickland (1986), "Dependence of Auroral Middle UV Emissions on the Incident Electron Spectrum and Neutral Atmosphere," *J. Geophys. Res.* **91**, 321.

**5.5** Decker, D.T., B. Basu, J.R. Jasperse, D.J. Strickland, J.R. Sharber, and J.D. Winningham (1995), "Upgoing Electrons in an Electron-Proton-Hydrogen Atom Aurora," *J. Geophys. Res.* **100**, 21,409.

**5.6** Jasperse, J.R., and B. Basu (1982), "Transport Theoretic Solutions for Auroral Proton and H Atom Fluxes and Related Quantities," *J. Geophys. Res.* **87**, 811.

**5.7** Strickland, D.J., D.L. Book, T.P. Coffey, and J.A. Fedder (1976), "Transport Equation Techniques for the Deposition of Auroral Electrons," *J. Geophys. Res.* **81**, 2755.

**5.8** Strickland, D.J., J.R. Jasperse, and J.A. Whalen (1983), "Dependence of Auroral FUV Emissions on the Incident Electron Spectrum and Neutral Atmosphere," *J. Geophys. Res.* **88**, 8051.

**5.9** Strickland, D.J., R.R. Meier, J.H. Hecht, and A.B. Christenson (1989), "Deducing Composition and Incident Electron Spectra from Ground Based Auroral Optical Measurements: Theory and Model Results," *J. Geophys. Res.* **94**, 13,527.

**5.10** Strickland, D.J., R.E. Daniell, J.R. Jasperse, and B. Basu (1993), "Transport-Theoretic Model for the Electron-Proton-Hydrogen Atom Aurora, 2. Model Results," *J. Geophys. Res.* **98**, 21,533.

## 6. Dates of development, authors, and sponsors

### 6.1 Dates:

1976 Original electron transport code for a one-constituent medium.

1982 Original proton-H-atom transport model and its analytic solutions for a one-constituent medium.

1983 Generalization of electron transport code to a multiconstituent medium and application to an auroral study.

1987 Study of a pure proton aurora with the proton-H-atom transport model.

1989 Application of electron transport code to an auroral study.

1990 Numerical proton-H-atom transport code for a multiconstituent medium.

1993 Electron-proton-H-atom transport code for a multiconstituent medium.

1995 Study of upgoing electrons in an electron-proton-hydrogen-atom aurora with transport code.

**6.2 Authors:** B. Basu and J. R. Jasperse, Phillips Laboratory/GPIM, Hanscom AFB, MA 01731; D. J. Strickland and R. E. Daniell, Computational Physics, Inc., 2750 Prosperity Avenue, Suite 600, Fairfax, VA 22031; D. T. Decker, Institute for Scientific Research, Boston College, Newton, MA 02159.

**6.3 Sponsors:** Air Force Office of Scientific Research (AFOSR), Defense Nuclear Agency (DNA), Defense Meteorological Satellite Program (DMSP), National Science Foundation (NSF), and Air Force Phillips Laboratory (PL).

### 7. Model codes and sources

The model is in the form of a research-type FORTRAN code and is not very user friendly. However, the authors frequently run the model in collaborative studies with experimentalists and other modelers. Anyone interested in such a study should contact J. R. Jasperse, Phillips Laboratory/GPIM, 29 Randolph Road, Hanscom AFB, MA 01731 (e-mail basub@plh.af.mil).

## TWO-CELL IONOSPHERIC CONVECTION MODEL

### 1. Model content

In the F-region ionosphere, the plasma drifts perpendicular to the magnetic field under the influence of the electric field such that  $V = \mathbf{E} \times \mathbf{B}/B^2$ . The electric field may be expressed in terms of a scalar electrostatic potential, and then electric equipotential lines indicate the instantaneous flow paths of the plasma. The F-region plasma motion is highly dependent on conditions in the interplanetary medium, particularly the interplanetary magnetic field (IMF) and the solar wind velocity. When the IMF is directed southward, most *in-situ* and remote sensing of the plasma motion at high latitudes in the F-region ionosphere confirms the existence of a two-cell circulation of the plasma, with antisunward flow at highest latitudes and sunward flow at lower latitudes largely confined to the regions of the auroral zone. This model provides an analytical expression for the electrostatic potential that describes a two-cell convection pattern and its first-order dependencies on the IMF. Specification of the potential distribution is achieved by defining a circular region (the polar cap) at high latitudes, within which the plasma flow is antisunward. The radius of the polar cap and the potential distribution across it determine the magnitude of the antisunward plasma flow. These variables may be specified by the user, or simple functional dependencies derived from observations from the Dynamics Explorer spacecraft and residing within the model algorithm may be invoked. Outside the polar cap, the sunward flow in the auroral region is determined by the distribution of the potential around the polar cap boundary and by a specification of the effective width of the auroral zone. These dependencies may also be fully specified by the user, or simple functional dependencies derived from DE-2 data may be invoked.

### 2. Model uncertainties

This model does not represent a synthesis of data in any way. It simply provides a tool by which major observed characteristics of the high-latitude convection pattern can be mimicked or by which specific observations of the electrostatic potential can be fit. The simple analytical functions that are employed do not allow convection features with scale sizes less than 10 deg in latitude or 6 hr in local time to be reproduced. The simple functional dependencies on the IMF presently provided by

the algorithms are based on a rather limited database from DE-2 and may differ significantly from those derived from other sources. Care should therefore be exercised when comparing derived results utilizing different specifications of the convection pattern. The model may presently be applied to conditions of southward IMF when confidence is high that a two-cell convection pattern exists. It is not applicable to times of weakly southward IMF or northward IMF when significant variations from the two-cell configuration are likely.

### 3. Basis of the model

Many studies of the high-latitude ionospheric convection describe a two-cell circulation (e.g., Foster, 1983; Heppner and Maynard, 1987). An original description of this convection configuration was given by Volland (1975). This model represents extensions to the functional forms given by Heelis et al. (1982) and dependencies of the driving parameters on the IMF given by Hairston and Heelis (1990). The model determines a distribution of electrostatic potential around a circular boundary defining the polar cap. This distribution is specified by a maximum and minimum potential, each of which occupies a local time extent dependent on the y component of the IMF. These local time regions are connected around the boundary using cubic splines through zero points that are also dependent on the y component of the IMF. The potential distribution inside this boundary is completed using a cubic spline that connects the specified boundary potentials with the location of a zero potential dependent on the y component of the IMF. Equatorward of the polar cap boundary, the electrostatic potential is specified by the segment of a gaussian with a half-width dependent on local time only.

### 4. Database

The functional forms utilized in the model are those that adapt most readily to the variety of two-cell convection patterns described by a number of workers. The dependence of the major driving parameters on the IMF was derived from fits to the derived potential distributions available from the DE-2 database.

### 5. Publication references

5.1 Volland, H. (1975), "Models of the Global Electric Fields within the Magnetosphere," *Ann. Geophys.* **31**, 159.

**5.2** Heelis, R.A., J.K. Lowell, and R.W. Spiro (1982), "A Model of the High-Latitude Ionospheric Convection Pattern," *J. Geophys. Res.* **87**, 6339.

**5.3** Foster, J.C. (1983), "An Empirical Electric Field Model Derived from Chatanika Radar Data," *J. Geophys. Res.* **88**, 981–987.

**5.4** Heppner, J.P. and N.C. Maynard (1987), "Empirical High Latitude Electric Field Models," *J. Geophys. Res.* **92**, 4467–4489.

**5.5** Hairston, M.R. and R.A. Heelis (1990), "A Model of the Ionospheric Convection Pattern for

Southward IMF Based on DE-2 Observations," *J. Geophys. Res.* **95**, 2333–2343.

## **6. Model codes and sources**

Functional forms that constitute the model are available in the published literature. Source codes that provide callable subroutines to provide the potential at any given location are available from R. A. Heelis, W. B. Hanson Center for Space Sciences, University of Texas at Dallas, Box 830688, Richardson, TX 75083-0688, USA (e-mail heelis@utdallas.edu).

## HEPPNER-MAYNARD ELECTRIC FIELD MODELS

### 1. Model content

The Heppner-Maynard electric field models of high-latitude convection electric fields were derived from the DE-2 satellite electric field measurements using a pattern recognition technique (Heppner and Maynard, 1987). The models are empirically derived potential patterns for various interplanetary magnetic field (IMF) orientations and for varying levels of  $K_p$ . The original patterns were presented for a nominal  $K_p$  level of 3+ with rules for changing size and potential strength as  $K_p$  varied. These patterns were parameterized using fits to spherical harmonic functions by Rich and Maynard (1989). The parameterized version covers  $K_p$  levels up through 7.

Convection patterns in the high-latitude ionosphere are very variable; however, basic signatures in the data tend to repeat for similar IMF conditions (Heppner, 1973). The goal was to develop a minimum set of patterns that would be representative of most conditions. Three patterns for IMF  $B_z$  south were derived. The BC pattern is representative of convection in the northern (southern) hemisphere for  $B_y$  negative (positive) conditions. In the BC and DE patterns, the polar cap convection is tilted to one side or the other. The A pattern is symmetric across the polar cap and is more often found in the sunlit hemisphere for appropriate IMF conditions.

For northward IMF, two levels of distortion of the southward IMF patterns were proposed. These patterns are qualitative but are conceptually useful. For pure  $B_z$  north, the pattern is more likely to be a four-cell pattern rather than the distorted two-cell. Both the distorted two-cell and the four-cell patterns are seen in the empirical models of Rich and Hairston (1994), which are derived from averaging DMSP ion drift data.

The advantage of a pattern recognition technique is that features near noon and midnight, which tend to shift back and forth in magnetic local time, retain their crispness of definition. A straight averaging technique tends to wash out detail in these regions because of the dynamics of these regions.

The Rich-Maynard parameterization of the Heppner-Maynard patterns requires the IMF  $B_z$  and  $B_y$  polarities to specify the patterns type and the  $K_p$

level. The output is a map of the potential. All patterns are given in magnetic-latitude/magnetic-local-time coordinates in a coordinate system corotating with the Earth. This is the natural system of the ionosphere. Conversion of these patterns into the inertial system, which is the natural system of the magnetospheric source, can be found in Maynard et al. (1995).

### 2. Model uncertainties and limitations

The model is valid at all altitudes in the ionosphere, assuming equipotential magnetic field lines. The projection of the electric fields along the magnetic field assumes that  $\mathbf{E} \times \mathbf{B} = 0$ . Above the ionosphere, field aligned electric fields at auroral latitudes may distort the projection back to the magnetospheric source.

The model is meant to represent the potential pattern for typical conditions for given model inputs. The model may or may not replicate the real convection pattern in any individual circumstance. This is especially true in the noon and midnight portions of the pattern, where considerable shifts in the pattern with magnetic local time are possible. Local mesoscale processes that may exist within the global system may distort areas of these global scale patterns.

The northward IMF patterns are conceptual only. The complexity of the patterns and the limited database do not provide the statistical significance that exists with the southward IMF patterns. For weakly northward IMF, the appropriate southward patterns for the given  $K_p$  conditions will approximate actual conditions. As the IMF turns more northward, the patterns evolve to the mildly distorted patterns and eventually toward the strongly distorted patterns or into a four-cell pattern.

### 3. Basis of model

The Heppner-Maynard patterns have been fitted to a spherical harmonic function based on Legendre polynomials. The resulting equipotential contours describe the plasma flow directions based on  $\mathbf{E} \times \mathbf{B} = 0$  and the convective flow  $\mathbf{E} \times \mathbf{B}/B^2$  in an incompressible fluid.

The global scale validity of the southward IMF models is attested to by the field-aligned current patterns derived by Rich and Maynard (1989) using the Heppner-Maynard patterns and the Hardy et al. (1987) conductivity patterns (averaging

patterns based on DMSP energetic electron precipitation statistical patterns). The divergence of the perpendicular currents calculated from these two empirical average patterns combines to produce reasonable facsimiles of the Iijima and Potemra (1976) average field-aligned current patterns based on Triad data.

#### 4. Database

The Heppner-Maynard patterns were derived from the double-probe electric field data from the DE-2 satellite covering the period from August 1981 to February 1983. This is a solarmax database.

#### 5. Publication references

**5.1** Hardy, D.A., M.S. Gussenhoven, R. Rais-trick, and W.J. McNeil (1987), "Statistical and Functional Representations of the Patterns of Auroral Energy Flux, Number Flux and Conductivity," *J. Geophys. Res.* **92**, 12,275.

**5.2** Heppner, J.P. (1972), "Polar Cap Electric Field Distributions Related to the Interplanetary Magnetic Field," *J. Geophys. Res.* **77**, 4877.

**5.3** Heppner, J.P., and N.C. Maynard (1987), "Empirical High-Latitude Electric Field Models," *J. Geophys. Res.* **92**, 4467.

**5.4** Iijima, T., and T.A. Potemra (1976), "The Amplitude Distribution of Field-Aligned Currents at Northern High Latitudes Observed by Triad," *J. Geophys. Res.* **81**, 2165.

**5.5** Maynard, N.C., W.F. Denig, and W.J. Burke (1995), "Mapping Ionospheric Convection Patterns to the Magnetosphere," *J. Geophys. Res.* **100**, 1713.

**5.6** Rich, F.J., and M. Hairston (1994), "Large-Scale Convection Patterns Observed by DMSP," *J. Geophys. Res.* **99**, 3827.

**5.7** Rich, F.J., and N.C. Maynard (1989), "Consequences of Using Simple Analytical Functions for the High-Latitude Convection Electric Field," *J. Geophys. Res.* **94**, 3697.

#### 6. Dates of development, authors, and sponsors

##### 6.1 Dates:

1976 Beginning of NASA Dynamics Explorer program.

1981 Satellites launched.

1987 Model completed and published.

1989 Parameterization of the models completed and published.

**6.2 Authors (principal):** J. P. Heppner, NASA Goddard Space Flight Center (now at Hughes STX, Lanham, MD); N. C. Maynard, NASA Goddard Space Flight Center and Phillips Laboratory (now at Mission Research Corporation, Nashua, NH); and F. J. Rich, Phillips Laboratory.

**6.3 Sponsors:** NASA, Phillips Laboratory, and Air Force Office of Scientific Research.

#### 7. Model codes and sources

The model is written in FORTRAN and is easily run on a workstation. It is available from F. J. Rich, Space Physics Division (Mail Code GPSG), Phillips Laboratory, 29 Randolph Road, Hanscom AFB, MA 01731 (e-mail rich@plh.af.mil).

## MILLSTONE HILL EMPIRICAL ELECTRIC FIELD MODEL, 1986

### 1. Model content

The Millstone Hill empirical electric field models are average patterns of ionospheric electric field derived from Millstone Hill incoherent scatter radar observations covering all local times at sub-auroral and auroral latitudes. Over 2.5 million radar measurements of plasma convection velocity, taken over the six-year interval from 1978–1984, were used in a variety of models. Bin-averaged convection models were generated from the radar data for each of the nine levels of an empirical high-latitude particle precipitation model derived from NOAA/ TIROS satellite observations (Foster et al., 1986). Data were binned, and averaged vectors calculated, each 0.5 hr of local time in 2-deg steps between 55 and 75 deg apex magnetic latitude. (Apex latitude is nearly identical to invariant latitude at Millstone Hill's longitude.) Averaged velocity vectors were determined completely independently in each cell. Assuming that the observed plasma velocities are the result of  $\mathbf{E} \times \mathbf{B}$  drifts in a time-stationary electric field, an analytical potential model with 12 (14) degrees of freedom in local time (latitude) was fit to each bin-averaged velocity pattern; these are available as coefficients of the B-spline expansion of the ionospheric electric field in magnetic latitude–local time coordinates. The methodology followed in constructing these empirical models accentuates the close relationship between electric field and conductances at ionospheric heights. The relationship, as presented in these models, was discussed by Kamide and Richmond (1987) and by Foster (1987). Averaged patterns of ionospheric conductances, derived in a similar fashion from the NOAA/TIROS database, were presented by Fuller-Rowell and Evans (1987); these were combined with the Millstone Hill electric field models to provide quantitative patterns of field-aligned currents by Foster et al. (1989). IMF sector dependence of auroral-latitude convection is represented by a set of models that binned the radar velocity observations by the 1-hr averaged values of IMF  $B_y$  and  $B_z$  components (Foster et al., 1986b). These IMF-dependent models were extended to polar latitudes through the inclusion of five years of data from the Sondrestrom incoherent scatter radar. The Millstone Hill empirical electric field models are used as electric field basis functions in studies of high-latitude electrody-

namics using the KRM (Richmond et al., 1988) and AMIE (Knipp et al., 1989) techniques.

### 2. Model uncertainties and limitations

The electric fields presented in these models describe average conditions on Millstone Hill's longitude (285°E), and electric field patterns determined here may reflect the unique Northern hemisphere relationship between solar-produced and auroral conductivities found in this sector. These are numerically averaged models and, as such, do not contain external biases due to data selection or interpretation. However, averaging smoothes boundaries (spatially) and reduces the extreme values in the patterns. The effects of individual substorms are not represented in these models, which average over such temporal/spatial effects.

### 3. Basis of model

Assume that the observed plasma velocities are the result of  $\mathbf{E} \times \mathbf{B}$  drifts in a time-stationary electric field.

### 4. Input to the model

Either the precipitation activity index or its associated value of  $K_p$  (Foster et al., 1986a) determines which averaged pattern is accessed. Alternately, models dependent on IMF  $B_y/B_z$  are available. The analytic subroutine provided with the model coefficients outputs field components or potential value at a user-specified latitude and local time.

### 5. Publication references

- 5.1** Evans, D.S., T.J. Fuller-Rowell, S. Maeda, and J. Foster (1987), "Specification of the Heat Input to the Thermosphere from Magnetospheric Processes Using TIROS/NOAA Auroral Particle Observations," *Adv. Astronaut. Sci.* **65**, 1649–1668.
- 5.2** Foster, J.C., J.M. Holt, R.E. Musgrove, and D.S. Evans (1986a), "Ionospheric Convection Associated with Discrete Levels of Particle Precipitation," *Geophys. Res. Letters* **13**, 656–659.
- 5.3** Foster, J.C. (1987a), "Radar-Deduced Models of the Convection Electric Field," *Quantitative Modeling of Magnetosphere-Ionosphere Coupling Processes*, pp. 71–76, edited by Y. Kamide, Kyoto Sangyo Univ. Publishers, Kyoto.

**5.4** Foster, J.C. (1987b), "Reply to Kamide and Richmond," *Geophys. Res. Letters* **14**, 160–161.

**5.5** Foster, J.C., J.M. Holt, R.G. Musgrove, and D.S. Evans (1986b), "Solar Wind Dependencies of High-Latitude Convection and Precipitation," *Proceedings of the Chapman Conference on Solar Wind-Magnetosphere Coupling*, edited by Y. Kamide and J. Slavin, pp. 477–494.

**5.6** Foster, J.C., T. Fuller-Rowell, and D.S. Evans (1989), "Quantitative Patterns of Large-Scale Field-Aligned Currents in the Auroral Ionosphere," *J. Geophys. Res.* **94**, 2555–2564.

**5.7** Fuller-Rowell, T., and D.S. Evans (1987), "Height-Integrated Hall and Pedersen Conductivity Patterns Inferred from the NOAA-TIROS Satellite Data," *J. Geophys. Res.* **92**, 7606–7618.

**5.8** Maeda, S., T.J. Fuller-Rowell, D.S. Evans, and J.C. Foster (1987), "Numerical Simulations of Thermospheric Disturbances Excited by Magnetospheric Energy Input," *Quantitative Modeling of Magnetosphere-Ionosphere Coupling Processes*, pp. 22–27, edited by Y. Kamide, Kyoto Sangyo Univ. Publishers, Kyoto.

**5.9** Kamide, Y., and A.D. Richmond (1987), "Comment on 'Ionospheric Convection Associated with Discrete Levels of Particle Precipitation,'" *Geophys. Res. Letters* **14**, 158–159.

**5.10** Knipp, D.J., A.D. Richmond, J.C. Foster, et al., Electrodynamic Patterns for September 19, 1984, *J. Geophys. Res.*, **94**, 16913-16923, 1989.

**5.11** Richmond, A.D., Y. Kamide, B.H. Ahn, S.I. Akasofu, D. Alcayde, M. Blanc, O. de la Beujardiere, D.S. Evans, J.C. Foster, E. Friis-Christensen, T.J. Fuller-Rowell, J.M. Holt, D. Knipp,

H.W. Kroehl, R.P. Lepping, R.J. Pellinen, C. Senior, and A.N. Zaitzev (1988), "Mapping Electrodynamic Features of the High-Latitude Ionosphere from Localized Observations: Combined Incoherent-Scatter Radar and Magnetometer Measurements for 1984 January 18–19," *J. Geophys. Res.* **93**, 5760–5776.

## **6. Dates of development, authors, and sponsors**

### **6.1 Dates:**

1986 Precipitation index/Kp models.

1986 IMF By/Bz models.

1988 Millstone/Sondrestrom merged models.

**6.2 Author (principal):** John Foster, Associate Director, MIT Haystack Observatory, Westford, MA.

**6.3 Sponsor:** U.S. National Science Foundation.

## **7. Model code**

FORTTRAN codes to generate full LT/latitude patterns of electrostatic potential or electric field components or magnitude have been distributed to the community or are available from the authors. The model has been deposited in the NCAR/CE-DAR database for research-community use.

## APL HIGH-LATITUDE CONVECTION MODEL

### 1. Model content

The Atmospheric and Ionospheric Remote Sensing group of the Johns Hopkins University Applied Physics Laboratory (APL) has developed an empirical model of high-latitude magnetospheric plasma convection. The principal product is the distribution of electrostatic potential in invariant latitude and MLT coordinates above  $\sim 50^\circ\Lambda$ . The contours of constant electrostatic potential delineate the plasma drift trajectories. The values of the electric field and drift velocity at any position can be directly inferred. The model is keyed to such indices of geomagnetic conditions as the IMF and Kp.

The model can be reduced to a set of coefficients that describe a series expansion of the potential in spherical harmonics. Equipped with these coefficients and the transformation formulas given below, the user can generate all convection parameters.

At the current stage of development, the most complete modeling has been done for the primary IMF dependencies, namely, IMF magnitude in the y-z plane (three levels) and orientation (45-deg step in IMF y-z clock angle). There is also a detailed solution for the IMF y-z clock angle dependencies under moderately disturbed conditions,  $2 < Kp < 3+$ .

### 2. Model uncertainties and limitations

**2.1** The model is statistical in nature and hence can only approximate real-time convection, which is known to be highly variable. For example, the transient effects associated with substorm phases cannot be reliably imaged.

**2.2** Beyond the effective latitudinal limits of radar coverage ( $65^\circ\text{--}85^\circ\Lambda$ ), the convection is partly solved by applying Laplace's condition,

$$\nabla^2\Phi = 0$$

subject to boundary conditions that include the assumption that the region below a reference latitude  $\Lambda_0$  is shielded from the convection electric field. The model can be expected to be less reliable outside the region of direct radar observations.

**2.3** The radar velocity coverage becomes sparse for more restricted conditions, e.g., small steps in IMF clock angle or Kp disturbance level. The indicial sorting intervals are selected for reliable mapping of the large-scale convection over as large a range of indicial variation as possible. Where the statistics are insufficient, a reduction in the quality of the results may be apparent.

**2.4** The geomagnetic field model of Baker and Wing (1989) was applied in the analysis. The field models in common usage can differ in latitude by several degrees.

### 3. Basis of the model

**3.1** The model is based on observations carried out with the coherent-scatter HF radar located at Goose Bay, Labrador, over the period September 1987–July 1993. This instrument measures the  $\mathbf{E} \times \mathbf{B}$  drift of F-region plasma at invariant latitudes greater than  $65^\circ\Lambda$ .

**3.2** To generate the model for a set of specified conditions, the line-of-sight velocity data are first sorted and averaged in 12-min UT bins. Two-dimensional vectors are generated by examining the variation of the line-of-sight velocity within MLT/latitude cells with UT. The vectors are then fitted to a polynomial expansion of the electrostatic potential distribution. The mapping of the potential is extrapolated to the high polar cap and lower latitude regions. Finally, the potential distribution is expressed as a series expansion in spherical harmonics.

**3.3** The product of the analysis is the set of coefficients required to solve for the electrostatic potential via the expression

$$\Phi(\mathbf{q}, \mathbf{f}) = \sum_{l=0}^{\infty} \sum_{-l}^l A_{lm} Y_{lm}(\mathbf{q}, \mathbf{f})$$

where the spherical harmonics are defined by

$$Y_{lm}(\mathbf{q}, \mathbf{f}) = \sqrt{\frac{2l+1}{4p} \frac{(l-m)!}{(l+m)!}} P_l^m(\cos \mathbf{q}) e^{imj}$$

and the effective colatitude is given by

$$\mathbf{q} = \frac{P}{(P/2 - \Lambda_0)} (P/2 - \Lambda)$$

where  $f$  is the MLT clock angle in radians measured from 0 MLT,  $\Lambda$  is the invariant latitude in radians, and  $\Lambda_0$  is a reference latitude in radians that is output by the model. The electric field and convection velocity can be solved from the relations

$$\mathbf{E} = -\nabla\Phi \text{ and } \mathbf{v} = (\mathbf{E} \times \mathbf{B}) / B^2$$

**3.4** The derivation of the model and the related analysis were described by Ruohoniemi and Greenwald (1995, 1996).

#### **4. Database**

The primary measurements of convection velocity were made with the Goose Bay HF radar. This instrument is located at 299.5°E longitude and 53.3°N latitude. It operates around the clock and completes an azimuthal scan of the F-region ionosphere north of the site every 2 min. The Goose Bay radar is part of a network of HF radars that have recently been installed at high latitudes as part of the SuperDARN initiative (Greenwald et al., 1995). The IMF data were culled from the records of the IMP8 spacecraft provided by several sources of geophysical data.

#### **5. Publication references**

**5.1** Baker, K.B., and S. Wing (1989), "A New Magnetic Coordinate System for Conjugate Studies of High Latitudes," *J. Geophys. Res.* **94**, 9139–9143.

**5.2** Greenwald, R.A., et al. (1995), "DARN/SuperDARN: A Global View of High-Latitude Convection," *Space Sci. Rev.* **71**, 763–796.

**5.3** Ruohoniemi, J.M., and R.A. Greenwald (1995), "Observations of IMF and Seasonal Effects in High-Latitude Convection," *Geophys. Res. Letters* **9**, 1121–1124.

**5.4** Ruohoniemi, J.M., and R.A. Greenwald (1996), "Statistical Patterns of High Latitude Convection Obtained from Goose Bay HF Radar Observations," *J. Geophys. Res.* **101**, 21,743–21,763.

#### **6. Dates of development, authors, and sponsors**

**6.1 Date:** 1995 Development of code to reduce archival Goose Bay HF radar velocity data to maps of high-latitude convection.

**6.2 Authors:** J. Michael Ruohoniemi and Raymond A. Greenwald.

**6.3 Sponsor:** The National Science Foundation.

#### **7. Model codes and sources**

The model, or portions thereof, can be readily acquired either in the form of global maps of the electrostatic potential or as sets of coefficients that describe expansions of the potential patterns in terms of spherical harmonics. A small package of IDL routines allows easy access to the outputs of the model in graphical or digital form. The inventory of currently available solutions was described in Sec. 1. Interested persons should contact the authors at [mike\\_ruohoniemi@jhuapl.edu](mailto:mike_ruohoniemi@jhuapl.edu) or [ray\\_greenwald@jhuapl.edu](mailto:ray_greenwald@jhuapl.edu).

## HWM EMPIRICAL WIND MODEL

### 1. Model content

The HWM (Horizontal Wind Model) provides an estimate of the climatological average meridional and zonal components of the atmospheric wind vector as a function of altitude, latitude, longitude, day of year, time of day, and solar and magnetic activity. Solar and magnetic activity variations are only included for the thermosphere. Solar diurnal and semidiurnal tides are included in the stratosphere and above, and annual and semiannual variations at all altitudes. Longitude and UT variations related to magnetic field control of energy input and drag forces are included in the thermosphere and stationary wave longitude variations in the lower atmosphere (7–90 km).

### 2. Model uncertainties and limitations

Solar activity variations are weak and not very clearly delineated by the data. Because of the sparsity of data between 130 and 220 km and concern with providing reasonable continuity through this region, a simplifying assumption of proportionality to exospheric winds was introduced in this region. Rapid changes in winds at high latitudes resulting from magnetic control are likely underestimated by the small number of harmonics used. Quasi-biennial variations in the lower atmosphere are not included. Longitude variations in the lower atmosphere were only represented by the nondivergent vector field and had to be dependent on gradient wind derivations. Meridional winds are assumed to be zero below 45 km. There appear to be unresolved discrepancies between measurement techniques in the meso-pause region, which are a difficulty for model generation at these altitudes.

Overall root mean square differences between data and model values are on the order of 100–150 m/sec in the high-latitude thermosphere and 50 m/sec or less at mid to low latitudes. Root mean square differences are 15 m/sec in the mesosphere and 10 m/sec in the stratosphere for zonal winds, and 10 and 5 m/sec, respectively, for meridional winds.

### 3. Basis of the model

The model represents spatial variations in the wind vector by an expansion in vector spherical harmonics, with each expansion coefficient represented by a Fourier series in universal time and/or day of year as appropriate, and with sim-

plified supplemental equations for solar activity and magnetic activity variations. The expansion involves two orthogonal vector fields, the divergence B field and the rotational C field. Above 200 km, the altitude variations of the wind components are each represented by an analog of the Bates formula as used for thermospheric temperature profiles. Below 200 km, the wind profiles are represented by a cubic spline between specified nodes, with first and second derivatives continuous across interior nodes. The variation of the wind at each node is represented by an independent spherical harmonic/Fourier expansion.

### 4. Database and input to the model

The primary data incorporated in the model depend upon altitude. For the thermosphere (Hedin et al., 1991a), these are satellite mass spectrometer (WATS on DE-2 and NATE on AE-E) and Fabry-Perot (FPI on DE-2) instruments, ground-based incoherent scatter radar, and ground-based Fabry-Perot optical instrumentation. In the esosphere/lower thermosphere (Hedin et al., 1996), data are included from a wide range of MF radar and meteor radar stations, rocketsondes, rocket grenade soundings, gradient winds from MSISE-90 (Hedin et al., 1991b), CIRA-86, and earlier data tabulations. In the stratosphere, the data include rocketsondes and rocket grenade soundings, CIRA-86, and some earlier data tabulations. In the troposphere, the model is essentially a recasting of CIRA-86. The influence of gradient wind estimates was minimized in favor of direct wind measurements whenever possible. In addition to position and time coordinates, the model (in the thermosphere) requires a three-month average and previous day value of the 10.7-cm solar flux index (at the earth) and either the daily Ap magnetic index or a prescribed history of 3-hr Ap indices.

### 5. Publication references

**5.1** Hedin, A.E., N.W. Spencer, and T.L. Killeen (1988), "Empirical Global Model of Upper Thermosphere Winds Based on Atmosphere and Dynamics Explorer Satellite Data," *J. Geophys. Res.* **93**, 9959–9989.

**5.2** Hedin, A.E., et al. (1991a), "Revised Global Model of Thermosphere Winds Using Satellite and Ground-Based Observations," *J. Geophys. Res.* **96**, 7657–7688.

**5.3** Hedin, A.E. , et al. (1991b), "Extension of the MSIS Thermosphere Model into the Middle and Lower Atmosphere," *J. Geophys. Res.* **96**, 1159–1172.

**5.4** Hedin A.E., et al. (1996), "Empirical Wind Model for the Upper, Middle and Lower Atmosphere," *J. Atmos. Terr. Phys.* **58**, 1421–1447.

## **6. Dates of development, authors, and sponsors**

### **6.1 Dates:**

1988 HWM87 satellite-based thermosphere only model.

1991 HWM90 satellite- and ground-based thermosphere model.

1996 HWM93 extension to lower atmosphere (no change in thermosphere).

**6.2 Author (principal):** Alan E. Hedin.

**6.3 Sponsor:** NASA.

## **7. Model codes and sources**

FORTRAN subroutines are available from the National Space Science Data Center Request Coordinator Office, NSSDC, Code 633, NASA Goddard Space Flight Center, Greenbelt, MD 20771, tel. 301/286-6695 (e-mail request@nssdca.gsfc. nasa.gov; http://nssdc.gsfc.nasa.gov).

## GLOBAL EMPIRICAL MODELS OF $T_e$

### 1. Model content

Satellite Langmuir probe measurements have been used extensively to devise global empirical models of F-region  $T_e$ , and sometimes  $N_e$ . The use of *in situ* measurements for this purpose offers many challenges, however, since orbital limitations and the limited duration of the databases make it difficult to separate spatial and temporal variations (altitude, latitude, local time, season, solar cycle, geomagnetic activity). Therefore, it is usually necessary to devise models that describe limited aspects of ionosphere structure at specific times, such as the latitudinal and local time structure at a fixed altitude, or the latitudinal structure at fixed local times and at specific seasons. It is particularly difficult to resolve the solar cycle variations, because satellite lifetimes are usually much shorter than a solar cycle, or even half of a cycle. One can sometimes combine two or three satellite databases to identify the solar cycle effects, but differences in the inclinations and altitudes of the orbits can make the task more difficult. The following describes several attempts to devise such models using Langmuir probe measurements from the Atmosphere Explorer (AE-C), ISIS-1, ISIS-2, and Dynamic Explorer (DE-2) satellites.

### 2. Global models for fixed altitudes

Brace and Theis (1981) employed measurements from Atmosphere Explorer-C, ISIS-1, and ISIS-2 to define the coefficients of global models that described the variations of  $T_e$  at several fixed altitudes (300, 400, 1400, and 2000 km) as a function of dip latitude and local time. Corresponding  $N_e$  models were not attempted because the much larger altitude and solar cycle variations of  $N_e$  tended to hide or distort the geographical variations. The circular orbit phase of AE-C provided data at altitudes of 300 and 400 km at solar minimum (1975–77), which became the basis for global  $T_e$  models for these altitudes. ISIS-2 provided measurements from a circular, near-polar orbit at 1400 km at low to moderate levels of solar activity in 1971–72. The  $T_e$  data were used to define the coefficients of a spherical harmonic model of  $T_e$  that described the latitude and local time variations at that altitude. The Langmuir probes on ISIS-1 provided data over a range of altitudes between 600 and 3600 km during the relatively weak solar maximum of 1969–70. The

$T_e$  data obtained between 2000 and 3600 km were averaged to define the latitude and local time variations at 3000 km.

### 3. Inverse relationship between $N_e$ and $T_e$ in the F region

During the elliptical orbit phase of the AE-C mission (1973–74), when the perigee was being maintained deep in the lower thermosphere,  $N_e$  and  $T_e$  were measured frequently down to about 130 km. Brace and Theis (1978) employed these data to investigate the relationship between  $N_e$  and  $T_e$  in the daytime ionosphere. (Actually, in that mission, the total ion density  $N_i$  was measured rather than  $N_e$ .) As expected,  $N_e$  and  $T_e$  were found to be inversely related, probably because the electron-ion cooling rate varies as the product of  $N_i$  and  $N_e$ , or  $N_e^2$ . This is the dominant process that determines  $T_e$  at altitudes near the F2 peak, whereas electron-neutral cooling becomes more important in the lower F region and E region. Since the elliptical phase of the mission lasted only through 1974 (low solar activity), the effect of the solar cycle on the inverse relationship between  $N_e$  and  $T_e$  could only be determined from later measurements in the circular orbit phase (1975–78) when the orbit was maintained between 250 and 400 km.

The above study of the inverse behavior of  $N_e$  and  $T_e$  applied only to the daytime ionosphere at latitudes below 50 deg. Higher latitudes were avoided to eliminate high-latitude electron heat sources. In general,  $N_e$  and  $T_e$  do not exhibit this inverse behavior in regions where there is no electron heat source (such as in the middle- and low-latitude nighttime ionosphere), since  $T_e$  and  $T_i$  cool to the gas temperature when the heat source is removed. For example, the nightside does exhibit inverse variations in  $N_e$  and  $T_e$  at geomagnetic latitudes between 40 and 60 deg. The electron heating is understood to be caused by heat conduction from the overlying plasmasphere, the time constant for cooling of which is longer than one night. The plasmasphere is also heated by collisions with magnetospheric ring current ions, and this heat causes an elevation of  $T_e$  at these latitudes, whereas the behavior of  $N_e$  is controlled by plasma and neutral gas transport processes.

### 4. Solar cycle effects on the relationship between $N_e$ and $T_e$

The AE-C mission (altitudes between 300–400 km) extended well into the period of rising solar

activity in 1977 and 1978, thus permitting the solar cycle variations of the F region to be investigated. Brace and Theis (1984) found little response of  $T_e$  to the rising solar activity, although  $N_e$  increased significantly. Apparently, increased effect of electron heating with increasing solar activity was canceled by increased electron-ion and electron-neutral cooling that goes along with increased ion and neutral gas densities.

The DE-2 Langmuir probe measurements allowed the above AE-C study to be extended through the following solar maximum (1981–83). Brace and Theis (1984) combined the AE-C and DE-2 data to study the effect of solar activity on the relationship between  $N_e$  and  $T_e$ . Their equation gives the ratio  $T_e/T_{e \text{ model}}$  as a function of  $F_{10.7}$ , where  $T_e$  represents individual measured values, and  $T_{e \text{ model}}$  refers to the Brace and Theis (1978) solar minimum model discussed above. At solar maximum,  $T_e/T_{e \text{ model}}$  is enhanced by nearly a factor of 2 relative to solar minimum values, although  $T_e$  itself did not change much during the solar cycle while  $N_e$  increased.

## 5. $T_e$ and $N_e$ models at solar maximum

The DE-2 satellite also provided global Langmuir probe measurements at solar maximum (1981–83). Brace and Theis (1990) used these data to devise an empirical model of the global variation (geomagnetic latitude and local time) of  $N_e$  and  $T_e$  at 400 km. Legendre polynomials through the fifth order were retained. Their comparisons of the DE-2 and AE-C models with the IRI model showed that the two exhibited similar solar cycle variations. They confirm the fact that  $T_e$  does not vary greatly with solar activity, but the  $N_e$  varies by nearly an order of magnitude from solar minimum to solar maximum.

## 6. Models of the latitude variation of $N_e$ and $T_e$ at fixed altitudes

An important limitation of the global models (Brace and Theis, 1990) is that the nature of the selected orbit provided insufficient coverage of all the important spatial and temporal variations of the ionosphere. This means that many aspects of

the latitudinal and local time structure could not be captured with high resolution; thus the 1990 global model was limited to fifth-order polynomial. Brace and Theis (1991) attempted to improve the latitudinal resolution by employing subsets of the DE-2 measurements that suppressed the local time, latitude, and seasonal variations. This allowed them to define a seventeenth-order polynomial model of the latitudinal variation of  $N_e$  and  $T_e$  at fixed altitudes and fixed local times that were allowed by the orbit. This was achieved by limiting the database to narrow altitude slices and single sweeps of perigee from pole to pole. Comparisons of the resulting high-resolution models with the corresponding  $T_e$  and  $N_e$  measurements themselves showed that most of the latitudinal structure that had previously been washed out in the fifth-order global models (Brace and Theis, 1990) was captured by the higher-order models.

## 7. Publication references

- 7.1** Brace, L.H., and R.F. Theis (1981), "Global Empirical Models of Ionospheric Electron Temperature in the Upper F-Region and Plasmasphere Based on In Situ Measurements from the Atmosphere Explorer-C, ISIS-2 Satellites," *J. Atmos. Terr. Phys.* **43**, 1317–1343.
- 7.2** Brace, L.H. and R.F. Theis (1978), "An Empirical Model of the Interrelationship of Electron Temperature and Density in the Daytime Thermosphere at Solar Minimum," *Geophys. Res. Letters* **5**, 275–278.
- 7.3** Brace, L.H. and R.F. Theis (1984), "Solar Cycle Effects upon the Relationship of  $N_e$  and  $T_e$  in the F-Region," *Adv. Space Res.* **4** (1), 89–91.
- 7.4** Brace, L.H. and R.F. Theis (1990), "Global Models of  $N_e$  and  $T_e$  at Solar Maximum Based on DE-2 Measurements," *Adv. Space Res.* **10** (11), 39–45.
- 7.5** Brace, L.H. and R.F. Theis (1991), "Empirical Models of the Latitudinal Variations of  $T_e$  and  $N_e$  in the Ionosphere at Solar Maximum," *Adv. Space Res.* **11** (10), 159–166.

## EMPIRICAL MODEL OF THE IONOSPHERIC ELECTRON AND ION TEMPERATURES

### 1. Model content

The empirical model provides electron temperatures  $T_e$  [K] and ion temperatures  $T_i$  [K] as a function of

- Altitude: 50–4000 km
- Attitude: dipole latitude,  $N_2$ ,  $O_2$ , O, NO
- Time: day count  $d$  (annual variation), magnetic local time  $\tau$
- Solar activity: solar flux  $F_{10.7}$  for quiet geophysical conditions ( $K_p \leq 3$ )

The electron and ion temperatures are obtained from the appropriate figures of Köhnlein (1986) at  $F_{10.7} = 84 \times 10^{-22} \text{ Wm}^{-2} \text{ H}\zeta^{-1}$  and  $K_p \leq 3$ :

Average temperature (time-independent): see Köhnlein (1986, Figs. 4 and 5),

$T_{e,i}$  vs altitude

Time-independent temperature (latitudinal): see Köhnlein (1986, Figs. 6–11),

$T_{e,i}$  vs altitude at  $f = 90^\circ, 45^\circ, 0^\circ, -90^\circ$

$T_{e,i}$  vs dipole latitude at discrete heights

Annual variation:

see Köhnlein (1986, Figs. 12–17),

$T_{e,i}$  vs altitude at equinox and solstice conditions ( $d=80, 173, 266, 356$ )

Comparison with data:  $T_{e,i}$  vs day count at discrete heights

$\Delta T_{e,i}$  (relative): dipole latitude vs day count at discrete heights

Diurnal variation:

see Köhnlein (1986, Figs. 18–25),

$T_{e,i}$  vs altitude at  $f = 0^\circ, 45^\circ$  and  $t = 0\text{h}, 6\text{h}, 12\text{h}, 18\text{h}$

Comparison with data:  $T_{e,i}$  vs magnetic local time at discrete heights and  $f = 0^\circ, 45^\circ$

$\Delta T_{e,i}$  (relative): dipole latitude vs magnetic local time at discrete heights

and superpositions thereof, i.e.,

Diurnal variation + relative annual variation

⇒

diurnal variation at a selected day of the year

Annual variation + relative diurnal variation

⇒

annual diurnal variation at a selected magnetic local time

### 2. Model uncertainties and limitations

The discrepancies between the model and the observations (used) are shown for the annual and diurnal variations in Köhnlein (1986, Figs. 13, 16, 20, 21, 23, 24). In general, the model agrees well with the observations.

The uncertainties of the model are mainly due to the uneven data coverage and the simplicity of the analytical approach (e.g., linearity, no longitudinal terms, no disturbed conditions).

Data from epochs not used in the database may show stronger deviations toward the model. This is especially true for disturbed geophysical conditions that are not considered in the model.

### 3. Basis of the model

The vertical and horizontal structures of the model are treated on an equal footing.

The electron and ion temperatures are expanded into spherical harmonics (Köhnlein, 1986, Eqs. 1–12) wherein the model coefficients depend on altitude, solar flux  $F_{10.7}$ , and geomagnetic index  $K_p$ .

Restricting the model to quiet geophysical conditions ( $K_p \leq 3$ ), the above coefficients depend linearly on  $F_{10.7}$ , whereas their height variations are expressed by cubic spline functions.

### 4. Database

The database of the model consists of observations by satellites, incoherent scatter stations, and rocket profiles covering the time interval 1964–1979 (Köhnlein, 1986, Table1; Brace and Theis, 1981).

### 5. Publication references

**5.1** Brace, L.H., and Theis, R.F. (1981), "Global Empirical Model of Ionospheric Electron Temperature in the Upper F-Region and Plasmasphere Based on In Situ Measurements from the Atmospheric Explorer-C, ISIS-1, and ISIS-2 Satellites," *J. Atmos. Terr. Phys.* **43**, 1317.

**5.2** Köhnlein, W. (1986), "A Model of the Electron and Ion Temperatures in the Ionosphere," *Planetary Space Sci.* **34** (7), 609–630.

## **6. Dates of development, authors, and sponsors**

**6.1 Date:** 1983.

**6.2 Author:** W. Köhnlein.

**6.3 Sponsors:** Deutsche Forschungsgemeinschaft and University of Bonn.

## **7. Model codes and sources**

The model was developed in FORTRAN code, specifically adapted to a CDC-computer. Because of the detailed graphical representation, Köhnlein (1986) can be used as a quick reference for ionospheric temperatures ( $T_e$ ,  $T_i$ ) at low solar fluxes ( $F_{10.7} \approx 84$ ) and quiet geophysical conditions ( $K_p \leq 3$ ) in the altitude interval 50–4000 km.

## PHOTOCHEMICAL EQUILIBRIUM MODEL FOR IONOSPHERIC CONDUCTIVITY

### 1. Model content

The photochemical equilibrium model of the high-latitude ionosphere calculates density profiles for four ions ( $N_2^+$ ,  $O_2^+$ ,  $NO^+$ , and  $O^+$ ) and electrons over the altitude range from 85 to ~220 km. The densities are then used to calculate Pedersen and Hall conductivities. The model takes account of photoionization, impact ionization due to energetic electron precipitation, and ionization due to resonantly scattered solar radiation, starlight, and recombination radiation. The model outputs the ion and electron density profiles, altitude profiles for the Hall and Pedersen conductivities, and height-integrated conductivities.

### 2. Model uncertainties and limitations

The model is based on the assumption of chemical equilibrium and, therefore, is valid only at the altitudes where transport processes are negligible. The model results are also sensitive to certain inputs, including the auroral electron energy flux and characteristic energy, and the adopted ion and electron temperatures.

### 3. Basis of the model

**3.1** The model is based on a numerical solution of the coupled continuity equations for the ions  $NO^+$ ,  $O_2^+$ ,  $N_2^+$ , and  $O^+$ , assuming chemical equilibrium conditions prevail. The coupled nonlinear equations are solved with an iterative procedure at the specified altitudes and times.

**3.2** The momentum equations are solved to obtain expressions for the Hall and Pedersen conductivities assuming steady-state conditions and neglecting spatial gradients. In calculating the appropriate collision frequencies, account is taken of ion collisions with the neutrals  $N_2$ ,  $O_2$ ,  $O$ ,  $N$ , and  $NO$ .

**3.3** The height-integrated conductivities are obtained by using a trapezoidal rule to integrate in height.

### 4. Model input parameters

The model requires the electron energy flux and characteristic energy of the auroral precipitation, the neutral densities and temperature, and the ion and electron temperatures. These inputs are described by empirical models if they are not specified.

### 5. Publication references

**5.1** C.E. Rasmussen, R.W. Schunk, and V.B. Wickwa (1988), "A Photochemical Equilibrium Model for Ionospheric Conductivity," *J. Geophys. Res.* **93**, 9831–9840.

### 6. Dates of development, authors, and sponsors

**6.1 Date:** 1988 Developed this year, but no improvements since then.

### 7. Model codes and sources

The model is in the form of a Fortran code, and it can be obtained from the lead author of the referenced publication.

## EMPIRICAL MODEL OF CONDUCTIVITIES

### 1. Model content

The global patterns of the integral energy flux and average energy of precipitating auroral electrons are used to determine height-integrated Hall and Pedersen conductivities as a function of corrected geomagnetic latitude (CGL) and magnetic local time (MLT) for a range of magnetospheric conditions parameterized by either Kp or by IMF Bz and Vsw (see "Auroral Electron and Ion Fluxes" on page 49 of this report).

### 2. Model uncertainties and limitations

**2.1** The individual statistical maps were constructed from anywhere between 0.2 and 3.8 million spectra (depending on the magnetospheric activity sort parameter), which were binned and averaged into a spatial grid (CGL  $\times$  MLT). By their very nature, statistical maps obscure the short-lived, small-scale-length precipitation features (Redus et al., 1988). Thus, these models are not expected to track the ionospheric conductivities (as determined by electron precipitation) throughout individual (sub)storms with high precision, but they do provide a reasonable measure of the gross variations in an average sense. Whether the Bz-Vsw maps resolve the short-lived, small-scale-length features more successfully than do the Kp maps has never been investigated, although they are expected to because the sort parameters are more directly tied to solar wind-magnetospheric coupling (hence electron precipitation), and the parameter space has a finer grid (30 Bz-Vsw maps vs 7 Kp maps).

**2.2** The steep gradient (with respect to CGL) in conductivity at the time-dependent equatorward and poleward auroral boundary introduces an intrinsic difficulty in predicting conductivities along a specified orbit trajectory in proximity to such boundaries (as is the case for auroral precipitation flux). An uncertainty of 2–4 deg in magnetic latitude in the boundary location can mean up to a factor of 2 difference in conductivity, depending on whether the trajectory is cutting through the oval or just skimming it.

### 3. Basis of the model

**3.1** This model is based on a compilation of statistical hemispherical maps of auroral electron precipitation derived from measurements made by Air Force particle detectors flown primarily on

the DMSP (and, to a lesser extent, P78-1) satellites under a wide range of magnetospheric conditions.

**3.2** These statistical maps were created from electron flux databases, which were separated according to the magnetic activity index Kp (Hardy et al., 1985) and according to the z component of the interplanetary magnetic field (Bz) and the solar wind speed (Vsw) (Brautigam et al., 1991). For the Kp models, the separation resulted in seven intervals of Kp: Kp = 0, 0<sup>+</sup>, Kp = 1-, 1, 1<sup>+</sup>, etc., up to Kp = 5-, 5, 5<sup>+</sup>, and for Kp  $\geq$  6-. For the Bz-Vsw models, each map was defined by a discrete point in the parameter space defined by ordered pairs of Bz = (-4.5, -2.2, -0.7, 0.7, 2.2, 4.5 nT) and Vsw = (346, 408, 485, 572, and 677 km/sec).

**3.3** The various maps were all created using the same spatial grid defined by CGL and MLT. The high-latitude region was separated into 30 zones in CGL between 50 and 90 deg and 48 0.5-hr zones in MLT. The zones in latitude are 2 deg wide between 50 and 60 deg and between 80 and 90 deg; they are 1 deg wide between 60 and 80 deg latitude. Although the nominal altitude of the DMSP satellites is 840 km, particle fluxes are mapped down the magnetic field lines to 110 km (base of the ionospheric E layer) before constructing the statistical maps.

**3.4** In each spatial element, and at each level of activity, the average flux value in each of the energy channels was determined. The resulting average spectra were extrapolated to 100 keV. The final spectra were integrated over energy (from 0.5 to 100 keV) to determine the average integral number flux and the average integral energy flux of the precipitating electrons in each spatial element. The average energy was calculated by dividing the integral energy flux by the integral number flux. The Hall and Pedersen conductivities were then determined from the average energy and energy flux.

**3.5** Finally, the conductivities were fit to Epstein functions, with the function coefficients published as a representation of the statistical maps: (1) Kp models (Hardy et al., 1987); and (2) Bz-Vsw models (McNeil and Brautigam, 1998).

### 4. Model input parameters

There is a version of the conductivity models that is driven by the magnetic activity index Kp, and one that is driven by a pair of parameters: the z

component of the interplanetary magnetic field (Bz) and solar wind speed (Vsw). One source for these parameters is the World Wide Web site <http://nssdc.gsfc.nasa.gov/omniweb>.

## 5. Publication references

**5.1** Brautigam, D.H., M.S. Gussenhoven, and D.A. Hardy (1991), "A Statistical Study on the Effects of IMF Bz and Solar Wind Speed on Auroral Ion and Electron Precipitation," *J. Geophys. Res.* **96**, 5525.

**5.2** Hardy, D.A., M.S. Gussenhoven, R. Raistrick, and W.J. McNeil (1987), "Statistical and Functional Representations of the Pattern of Auroral Energy Flux, Number Flux, and Conductivity," *J. Geophys. Res.* **92**, 12,275.

**5.3** Hardy, D.A., M.S. Gussenhoven, and E. Holeman (1985), "A Statistical Model of Auroral Electron Precipitation," *J. Geophys. Res.* **90**, 4229.

**5.4** Redus, R.H., M.S. Gussenhoven, D.A. Hardy, and D.H. Brautigam (1988), "Deviations from the Average Patterns of Auroral Ion Precipitation," *Physics of Space Plasmas (1987)*, Vol.7, edited by T. Chang, G.B. Crew, and J.R. Jasperse, Scientific Publishers, Inc.

## 6. Dates of development, authors, and sponsors

**6.1 Dates:** 1985–1991      Development of conductivity models.

**6.2 Authors:** D.H. Brautigam, M.S. Gussenhoven, D.A. Hardy, E. Holeman, W.J. McNeil, R. Raistrick, and R.H. Redus.

**6.3 Sponsor:** Air Force Research Laboratory/VSBS.

## 7. Model codes and sources

The model code for Hall and Pedersen conductivities is identical to that described in the "Auroral Electron and Ion Fluxes" model.

**7.1** The simplest package of models is a set of FORTRAN subroutines for each species (electron; ion) and for each parameterized model (Kp; Bz and Vsw) which contain the Epstein coefficients for the functional forms of the various computed quantities (integral number flux, integral energy flux, average energy, and conductivities). These subroutines return a specified average quantity for a given model parameter and magnetic coordinates (CGL, MLT). They are available on PC diskettes. Contact D.H. Brautigam, AFRL/VSBS, 29 Randolph Road, Hanscom AFB, MA 10731 (e-mail [brautigam@plh.af.mil](mailto:brautigam@plh.af.mil)).

**7.2** These subroutines (7.1) are embedded within AF-Geospace, where they may be run in conjunction with a number of other options via an interactively driven graphical interface. AF-Geospace currently runs on UNIX-based Silicon Graphics workstations but is being ported to a Dec-Alpha workstation and will eventually run on Microsoft NT workstations. Contact G.P. Ginet, AFRL/VSBS, 29 Randolph Road, Hanscom AFB, MA 10731 (e-mail [ginet@plh.af.mil](mailto:ginet@plh.af.mil)).

## AURORAL ELECTRON AND ION FLUXES

### 1. Model content

Auroral particle (electron and ion) integral number flux, integral energy flux, and average energy are specified as a function of corrected geomagnetic latitude (CGL) and magnetic local time (MLT) for a range of magnetospheric conditions parameterized by either  $K_p$  or by IMF  $B_z$  and  $V_{sw}$ . From these statistical auroral flux maps, the number and energy flux precipitating over the entire auroral oval can be estimated for periods spanning weak to strong magnetic activity.

### 2. Model uncertainties and limitations

**2.1** The individual statistical maps were constructed from anywhere between 0.2 and 3.8 million spectra (depending on the magnetospheric activity sort parameter), which were binned and averaged into a spatial grid (CGL  $\times$  MLT). By their very nature, statistical maps obscure the short-lived, small-scale-length features (Redus et al., 1988). Thus, these models are not expected to track the auroral particle precipitation throughout individual (sub)storms with high precision, but they do provide a reasonable measure of the gross variations in the auroral oval in an average sense. Whether the  $B_z$ - $V_{sw}$  maps resolve the short-lived, small-scale-length features more successfully than do the  $K_p$  maps has never been investigated, although they are expected to because the sort parameters are more directly tied to solar wind-magnetospheric coupling, and the parameter space has a finer grid (30  $B_z$ - $V_{sw}$  maps vs 7  $K_p$  maps).

**2.2** The steep gradient (with respect to CGL) in auroral precipitation flux at the time-dependent equatorward and poleward auroral boundary introduces an intrinsic difficulty in predicting fluxes along a specified orbit trajectory in proximity to such boundaries. Even though the hemispheric number and energy flux inputs may be well modeled, an uncertainty of 2–4 deg in magnetic latitude in the boundary location can mean up to an order of magnitude difference in local flux, depending on whether the trajectory is cutting through the oval or just skimming it.

### 3. Basis of the model

**3.1** This model is based on a compilation of statistical hemispherical maps of auroral ion and electron precipitation derived from measurements

made by Air Force particle detectors flown primarily on the DMSP (and, to a lesser extent, P78-1) satellites under a wide range of magnetospheric conditions.

**3.2** These statistical maps were created from particle flux databases, which were separated according to the magnetic activity index  $K_p$  for both electrons (Hardy et al., 1985) and ions (Hardy et al., 1989) and according to the  $z$  component of the interplanetary magnetic field ( $B_z$ ) and the solar wind speed ( $V_{sw}$ ) for both electrons and ions (Brautigam et al., 1991). For the  $K_p$  models, the separation resulted in seven intervals of  $K_p$ :  $K_p = 0, 0^+, K_p = 1-, 1, 1^+$ , etc., up to  $K_p = 5-, 5, 5^+$ , and for  $K_p \geq 6-$ . For the  $B_z$ - $V_{sw}$  models, each map was defined by a discrete point in the parameter space defined by ordered pairs of  $B_z = (-4.5, -2.2, -0.7, 0.7, 2.2, 4.5 \text{ nT})$  and  $V_{sw} = (346, 408, 485, 572, \text{ and } 677 \text{ km/sec})$ .

**3.3** The various maps were all created using the same spatial grid defined by CGL and MLT. The high-latitude region was separated into 30 zones in CGL between 50 and 90 deg and 48 0.5-hr zones in MLT. The zones in latitude are 2 deg wide between 50 and 60 deg and between 80 and 90 deg; they are 1 deg wide between 60 and 80 deg latitude. Although the nominal altitude of the DMSP satellites is 840 km, particle fluxes are mapped down the magnetic field lines to 110 km (base of the ionospheric E layer) before constructing the statistical maps.

**3.4** In each spatial element and at each level of activity, the average flux value in each of the energy channels was determined. The resulting average spectra were extrapolated to 100 keV. The final spectra were integrated over energy to determine the average integral number flux and the average integral energy flux of the precipitating electrons and ions in each spatial element. The average energy was calculated by dividing the integral energy flux by the integral number flux.

**3.5** Finally, these average quantities were fit to Epstein functions, with the tables of function coefficients published as a representation of the statistical maps. These quantities and the references defining their representations are as follows: (1)  $K_p$  models (electrons): integral number and energy flux (Hardy et al., 1987); (2)  $K_p$  models (ions): average energy (McNeil and Brautigam, 1998), integral number, and energy flux (Hardy et al., 1987); and (3)  $B_z$ - $V_{sw}$  models (electrons and ions): average energy, integral

number, and energy flux (McNeil and Brautigam, 1998).

#### 4. Model input parameters

There is a version of the auroral model that is driven by the magnetic activity index Kp, and one that is driven by a pair of parameters: the IMF Bz and solar wind speed Vsw. One source for these parameters is the World Wide Web site <http://nssdc.gsfc.nasa.gov/omniweb>.

#### 5. Publication references

**5.1** Brautigam, D.H., M.S. Gussenhoven, and D.A. Hardy (1991), "A Statistical Study on the Effects of IMF Bz and Solar Wind Speed on Auroral Ion and Electron Precipitation," *J. Geophys. Res.* **96**, 5525.

**5.2** Hardy, D.A., W.J. McNeil, M. S. Gussenhoven, and D. Brautigam (1991), "A Statistical Model of Auroral Ion Precipitation: 2. Functional Representation of the Average Patterns," *J. Geophys. Res.* **96**, 5539.

**5.3** Hardy, D.A., M.S. Gussenhoven, and D. Brautigam (1989), "A Statistical Model of Auroral Ion Precipitation," *J. Geophys. Res.* **94**, 370.

**5.4** Hardy, D.A., M.S. Gussenhoven, R. Raistrick, and W. J. McNeil (1987), "Statistical and Functional Representations of the Pattern of Auroral Energy Flux, Number Flux, and Conductivity," *J. Geophys. Res.* **92**, 12,275.

**5.5** Hardy, D.A., M.S. Gussenhoven, and E. Holeman (1985), "A Statistical Model of Auroral Electron Precipitation," *J. Geophys. Res.* **90**, 4229.

**5.6** McNeil, W.J., and D.H. Brautigam (1998), AFRL Technical Report (to be published).

**5.7** Redus, R.H., M.S. Gussenhoven, D.A. Hardy, and D.H. Brautigam (1988), "Deviations

from the Average Patterns of Auroral Ion Precipitation," *Physics of Space Plasmas* (1987), Vol.7, edited by T. Chang, G.B. Crew, and J.R. Jasperse, Scientific Publishers, Inc.

#### 6. Dates of development, authors, and sponsors

**6.1 Dates:** 1985–1998 Development of auroral models.

**6.2 Authors:** D.H. Brautigam, M.S. Gussenhoven, D.A. Hardy, E. Holeman, W.J. McNeil, R. Raistrick, and R.H. Redus.

**6.3 Sponsor:** Air Force Research Laboratory/VSBS.

#### 7. Model codes and sources

**7.1** The simplest package of models is a set of FORTRAN subroutines for each species (electron; ion) and for each parameterized model (Kp; Bz and Vsw) which contain the Epstein coefficients for the functional forms of the various computed quantities (integral number flux, integral energy flux, average energy, and conductivities). These subroutines will return a specified average quantity for a given model parameter and magnetic coordinates (CGL, MLT). They are available on PC diskettes. Contact D.H. Brautigam, AFRL/VSBS, 29 Randolph Road, Hanscom AFB, MA 10731 (e-mail [brautigam@plh.af.mil](mailto:brautigam@plh.af.mil)).

**7.2** These subroutines (7.1) are embedded within AF-Geospace, where they may be run in conjunction with a number of other options via an interactively driven graphical interface. AF-Geospace currently runs on UNIX-based Silicon Graphics workstations but is being ported to a Dec-Alpha workstation and will eventually run on Microsoft NT workstations. Contact G.P. Ginet, AFRL/VSBS, 29 Randolph Road, Hanscom AFB, MA 10731 (e-mail [ginet@plh.af.mil](mailto:ginet@plh.af.mil)).

## WBMOD IONOSPHERIC SCINTILLATION MODEL (NWRA), 1995

### 1. Model content

NorthWest Research Associates (NWRA) has developed an empirical model of the irregularities in F-layer plasma density which produce radio-wave scintillation. Based mainly on direct measurement of intensity and phase scintillation, primarily from the Defense Nuclear Agency (DNA) Wide-Band Satellite Experiment, the scintillation model is incorporated in a computer program called WBMOD. Development of the model initially (Fremouw and Lansinger, 1981; Fremouw and Secan, 1984) was sponsored by DNA. Because of Wide-Band's sun-synchronous orbit and a limited number of observing sites, the early version of WBMOD did not fully reproduce the observed temporal and spatial variations of scintillation (Basu et al., 1988). Recently, the model was upgraded by ingesting high-latitude scintillation data from DNA's Hilat and Polar BEAR satellites and the time-continuous equatorial scintillation database of the Geophysics Directorate of Phillips Laboratory (PL/GD). These model upgrades (Secan and Bussey, 1994; Secan et al, 1995) have been executed by NWRA and were sponsored by PL/GD with the support of HQ Air Weather Service. In addition to scintillation observations, WBMOD incorporates a modified version of the phase-screen propagation theory of Rino (1979). For two-way propagation, the theory is augmented by the work of Fremouw and Ishimaru (1992). The irregularity model contains statistical descriptions of their anisotropy in geomagnetic coordinates and their spatial power spectrum, the latter characterized by means of an outer scale, a power-law spectral index, and the height-integrated power spectral density (psd), CkL, at a cross-field scale size of 1 km/cycle. The occurrence statistics of the most variable of these parameters, CkL, are modeled by means of a probability density function (pdf), the relevant moments of which are expressed as functions of geomagnetic latitude, longitude, local time of day, season, solar-cycle epoch, and planetary geomagnetic activity index. The irregularities are taken to drift with the background F layer. For an operating scenario (location, time, operating frequency, etc.) specified by the user, WBMOD outputs signal-statistical parameters that quantify phase and intensity scintillation. The phase spectrum is characterized by its power-law spectral index  $p$  and its psd  $T$  at a fluctuation frequency of 1 Hz. The rms phase fluctuation  $\sigma\phi$  for a time in-

terval specified by the user is computed as the square root of the integral of the spectrum. Intensity scintillation is quantified by the normalized (by the mean) standard deviation  $S_4$  of power, which also is converted to a dB scintillation index.

### 2. Model uncertainties and limitations

**2.1** The observations on which WBMOD is based were carried out at VHF, UHF, and L bands. The propagation theory that it incorporates is valid down to about 100 MHz (somewhat less at high elevation angles) and improves with increasing frequency.

**2.2** The irregularities are characterized by a single-regime power-law spatial spectrum, although spectra with at least two power-law regimes are known to exist at both auroral and equatorial latitudes.

**2.3** The high-latitude portion of the model has been well tested only at auroral latitudes, and deficiencies are likely in the polar cap. At auroral latitudes, testing has been without benefit of data from the Russian sector.

**2.4** The model's description of the coupled seasonal and longitudinal dependence of equatorial scintillation may suffer from sparse data and incomplete understanding of the relevant geophysical drivers.

**2.5** Versions 12, 13.00, and 13.01 output the SI index of Whitney et al. (1969) as an auxiliary (dB) intensity scintillation index. Since SI depends upon record length, the standard deviation of dB intensity is output instead of SI in Version 13.02.

**2.6** WBMOD is a climatological model. In view of the patchiness and day-to-day variability of scintillation, its outputs may differ considerably from measurements at a given place on a given day.

### 3. Basis of the model

**3.1** The model is based on multi-frequency scintillation measurements. The data were acquired at a variety of ground stations, which recorded scintillation of radio signals from low-orbiting and geostationary satellites.

**3.2** The scintillation data were translated to turbulence strengths of the irregularities by means of the phase-screen theory for weak scattering from irregularities with a power-law spectrum (Rino, 1979). The turbulence strength of the irregularities is characterized by the height-integrated psd at a

cross-field wave number corresponding to 1-km scale size. The irregularity spectrum is defined by an outer scale and a power-law spectral index. An empirical model of irregularity anisotropy and its variations is incorporated.

**3.3** The global irregularity model is used to specify scintillation parameters. Transformation from spatial to temporal statistics is based on scan of the line of sight and appropriate models of ionospheric drift.

#### 4. Database

**4.1** The primary data employed are intensity and phase scintillation measurements at VHF, UHF, and L band (with an S-band phase reference) carried out at Poker Flat, AK; Stanford, CA; Ancon, Peru; and Kwajalein, Marshall Islands in the WideBand experiment.

**4.2** More recently, data from the DNA HiLat and Polar BEAR Satellite experiments have been employed. Specifically, VHF and UHF phase (with an L-band reference) and intensity data recorded at Bellevue, WA; Tromso, Norway; Ft. Churchill, Manitoba; and Sondre Stromfjord, Greenland have been used.

**4.3** The foregoing have been augmented with intensity measurements performed by PL/GD at L band on Ascension Island in the Atlantic and at VHF in Manila, Phillipines, and Huancayo, Peru. Similar VHF data from Narssarsuaq, Greenland (Basu, 1975), have been applied to the question of seasonal variation at high latitudes.

#### 5. Publication references

**5.1** Basu, Sa., E. MacKenzie, and Su. Basu (1988), "Ionospheric Constraints on VHF/UHF Communications Links During Solar Maximum and Minimum Periods," *Radio Sci.* **23**, 363.

**5.2** Basu, Su. (1975), "Universal-Time/Seasonal Variations of Auroral-Zone Magnetic Activity and VHF Scintillations," *J. Geophys. Res.* **80**, 4725–4728.

**5.3** Fremouw, E.J., and A. Ishimaru (1992), "Intensity Scintillation Index and Mean Apparent Radar Cross Section on Monostatic and Bistatic Paths," *Radio Sci.* **27**, 539–543.

**5.4** Fremouw, E.J., and J.M. Lansinger (1981), "A Computer Model for High-Latitude Phase Scintillation Based on Wideband Satellite Data from Poker Flat," Defense Nuclear Agency, Washington, DC, Rept. DNA5686F.

**5.5** Fremouw, E.J., and J.A. Secan (1984), "Modeling and Scientific Application of Scintillation Results," *Radio Sci.* **19**, 87–694.

**5.6** Rino, C.L. (1979), "A Power-law Phase-screen Model for Ionospheric Scintillation: 1, Weak Scatter," *Radio Sci.* **14**, 1135–1145.

**5.7** Secan, J.A., and R.M. Bussey (1994), "An Improved Model of High-latitude F-Region Scintillation (WBMOD Version 13)," Phillips Lab., Hanscom AFB, MA, Rept. PL-TR-94-2254.

**5.8** Secan, J.A., R.M. Bussey, E.J. Fremouw, and Sa. Basu (1995), "An Improved Model of Equatorial Scintillation," *Radio Sci.* **30**, 607–617.

**5.9** Whitney, H.E., J. Aarons, and C. Malik (1969), "A Proposed Index for Measuring Ionospheric Scintillations," *Planetary Space Sci.* **17**, 1069–1073.

#### 6. Dates of development, authors, and sponsors

##### 6.1 Dates:

1981 Original high-latitude WMOD.  
 1984 Extension to equatorial latitudes.  
 1986 Extension to middle latitudes.  
 1994 Improvement at high latitudes.  
 1994 Improvement at middle latitudes.  
 1993, 1995 Improvements at equatorial latitudes.

**6.2 Authors (principal):** Edward J. Fremouw, NWRA President and Senior Research Scientist, and James A. Secan, NWRA Research Scientist.

**6.3 Sponsors:** Defense Nuclear Agency (now Defense Special Weapons Agency) of the U.S. Department of Defense, and Phillips Laboratory of the USAF Materiel Command.

#### 7. Model codes and sources

The evolution of WBMOD traced herein refers to the "research" versions developed by NWRA under contracts from DNA and Phillips Laboratory. Users interested in obtaining a copy should address requests to J.A. Secan (e-mail jim@nwra.com) or E.J. Fremouw (e-mail ed@nwra.com) at NWRA, P.O. Box 3027, Bellevue, WA 98009, tel. 425/644-9660. NWRA has devised specialized versions for the USAF Air Weather Service. Parties interested in versions tailored for particular applications should visit <http://www.nwra.com>, or contact Mr. Secan or Dr. Fremouw.

## MODEL OF THE TROUGH IN THE HIGH-LATITUDE F LAYER

### 1. Model content

MLAT/MLT boundaries occur in the high-latitude ionosphere that separates regions where there are macroscopic changes in F-layer electron density. These boundaries, which are often stable for many hours UT, are formed by the convection pattern and the auroral oval.

### 2. Model uncertainties and limitations

The model describes only foF2, so that hmF2 and the shape of the altitude profile must come from the parameterized USU model or from some empirical model. In addition, the model is uncertain about the merging of the afternoon trough with the mid-latitude ionosphere in the hours before midnight. A further uncertainty is the daytime trough in the morning sector from ~0600 to 1100 MLT, which is variable and poorly defined.

### 3. Basis of model

**3.1** This is an empirical model derived from data from a dense network of ionospheric sounders during winter at solar maximum.

**3.2** The first part is a daytime trough in the afternoon sector. The equatorward boundary of this trough separates the high-density daytime F layer from the depleted and disturbed F-region plasma. This is nighttime plasma that is transported sunward by the convection pattern. This trough is well defined and very persistent, extending as a spiral from about 1300 MLT until nearly midnight. The equatorward edge is the boundary of the convection pattern. At this edge, foF2 decreases exponentially with increasing MLAT over a nominal range of 3 deg to a nominal minimum value 2.5 times smaller than at the edge. However, foF2 remains constant over a range of 2 deg MLAT, where it is terminated by the auroral F layer.

**3.3** The second part is a post-midnight trough extending from midnight to dawn at nearly constant MLAT. This trough is defined by its minimum, which is the juncture between the normal nighttime mid-latitude F layer that decreases with latitude, and the auroral F layer that increases with latitude to form the poleward trough wall. As defined from its minimum, the trough increases in

foF2 with increasing latitude as  $\exp(\Lambda/3.7 \text{ deg})$ . It increases equatorward from the minimum with decreasing latitude as  $\exp(\Lambda/16 \text{ deg})$  with the mid-latitude F layer. The location and value of the minimum are determined by the intersection of these two regions, which vary independently. If not measurable directly, they are given by the boundary of the auroral oval and of the mid-latitude F layer, the latter given by the URSI coefficients.

### 4. Model input parameters

**4.1** If not measurable directly, the equatorward edge of the afternoon trough is taken from the Heppner-Maynard model, and foF2 at the equatorward edge, from the URSI coefficients.

**4.2** If not measurable directly, the post-midnight trough minimum is given by the boundary of the auroral oval and of the mid-latitude F layer by the URSI coefficients.

### 5. Publication references

**5.1** Whalen, J.A. (1987), "The Daytime F Layer Trough Observed on a Macroscopic Scale," *J. Geophys. Res.* **92**, 2571.

**5.2** Whalen, J.A. (1989), "The Daytime F Layer Trough and Its Relation to Ionospheric-Magnetospheric Convection," *J. Geophys. Res.* **94**, 17,169.

**5.3** Sojka, J.J., R.W. Schunk, and J.A. Whalen (1990), "The Longitude Dependence of the Day-side F-Region Trough: A Detailed Model-Observation Comparison," *J. Geophys. Res.* **95**, 15,275.

### 6. Dates of development, authors, and sponsors

**6.1 Dates:** 1985–1990.

**6.2 Author:** J.A. Whalen.

**6.3 Sponsor:** Air Force Geophysics Laboratory.

### 7. Model codes and sources

This daytime trough is incorporated in the High Latitude Ionospheric Specification Model.

## GPS EIGHT-COEFFICIENT TEC MODEL

### 1. Model content

The GPS (or Klobuchar) TEC model was originally developed in the late 1970s to provide an estimate of the ionospheric range delay for single-frequency users of the Global Positioning System (GPS). Because of very severe restrictions on the amount of data that could be transmitted as part of the GPS navigation message, the model attempts to represent the global ionosphere using only eight coefficients. These coefficients were derived from the Bent model and are functions of time of year and solar activity (represented by  $F_{10.7}$ ). Despite the model's computational simplicity, it performs remarkably well, with a root mean square (RMS) error of about 50%.

For a specified location, line of sight, time of day, day of the year, and solar activity level ( $F_{10.7}$ ), the model provides the ionospheric slant TEC (in terms of the group delay at 1.57542 GHz).

### 2. Model uncertainties and limitations

The most obvious limitation of the model is its reliance on only eight coefficients to represent the global ionosphere. It makes no attempt to model the equatorial anomaly or the highly dynamic high-latitude ionosphere.

### 3. Basis of the model

The GPS Eight-Coefficient Model was obtained by performing least-squares fits to vertical TEC computed from the Bent model. Since the Bent model's own coefficients are provided at 10-day intervals throughout the year, the GPS model was organized in the same way. The diurnal variation is described as a half cosine (actually calculated by its truncated Taylor series) for the daytime TEC and a constant value for the nighttime TEC. The amplitude and period of the half cosine are each described by a cubic equation in geomagnetic latitude (accounting for the eight coefficients broadcast in the GPS navigation message).

The conversion from vertical TEC to slant TEC is accomplished by multiplication by an obliquity factor that assumes a constant ionospheric height of 350 km. Conversion from the geodetic coordinates of the ionospheric intersection point to the geomagnetic coordinates required by the model is accomplished using approximate formulae.

### 4. Model input parameters

As implemented in a typical single-frequency GPS receiver, the inputs are the universal time (UT), the user's approximate location in geodetic coordinates, the azimuth and elevation of the line of sight, and the eight coefficients broadcast in the GPS navigation message. When used as a stand-alone model, it also requires the day of the year and solar activity level ( $F_{10.7}$ ). The stand-alone model can provide vertical TEC and slant TEC, as well as vertical and slant group delay.

### 5. Publication references

**5.1** Klobuchar, J.A. (1986), "Design and Characteristics of the GPS Ionospheric Time Delay Algorithm for Single Frequency Users," *Proceedings of PLANS '86*, Las Vegas, NV, pp. 280–286.

**5.2** Klobuchar, J.A. (1987), "Ionospheric Time-Delay Algorithm for Single Frequency GPS Users," *IEEE Transactions on Aerospace and Electronic Systems* **AES-23** (3), 325–331.

**5.3** Spilker, J.J. (1996), "GPS Navigation Data," *Global Positioning System: Theory and Applications*, Vol. I, edited by B.W. Parkinson and J.J. Spilker, AIAA, Reston, VA, pp. 121–176.

### 6. Dates of development, authors, and sponsors

**6.1 Date:** Late 1970s.

**6.2 Author:** John R. Klobuchar.

**6.3 Sponsor:** Air Force Geophysics Laboratory (AFGL), which is now a part of the Air Force Research Laboratory (AFRL).

### 7. Model codes and sources

Although the mathematical formulae of the model have been published in the references cited above, the tables of the eight coefficients for each 10-day period and each level of solar activity are not publicly available. A master set is maintained at AFRL and at the GPS Control Segment, which broadcasts the appropriate coefficients as part of the GPS navigation message.

## THE CPI TEC MODEL

### 1. Model content

The CPI TEC model for single-frequency GPS users was developed to replace the GPS Eight-Coefficient Model (Klobuchar Model). The CPI model is actually a three-dimensional model of the ionosphere similar to PIM but with additional environmental parameters, specifically a set of longitude-dependent parameters describing the equatorial vertical drift and thermospheric winds that control much of the day-to-day variability of the ionosphere.

The model takes advantage of the enormous computing power available in even handheld devices now available. The model provides slant TEC (in terms of the group delay at 1.57542 GHz) along the lines of sight to GPS satellites.

### 2. Model uncertainties and limitations

Although capturing more of the spatial structure of the ionosphere than the GPS Eight-Coefficient Model, the accuracy of the model is dependent on timely measurements of the equatorial vertical drift (for low latitudes) and/or the thermospheric winds (for mid latitudes). The model does not attempt to capture the dynamic state of the high-latitude ionosphere.

### 3. Basis of the model

Like its cousin PIM, the CPI GPS model is a parameterization of diurnally reproducible runs of the AFRL Global Theoretical Ionospheric Model (GTIM). Unlike PIM, however, the geophysical parameters include not only solar activity but also the equatorial vertical drift (which drives the formation of the equatorial anomaly) and the thermospheric winds (which control much of the variability of the mid-latitude ionosphere).

The output of GTIM is represented by an expansion in terms of Empirical Orthonormal Functions (EOFs) derived from a representative subset of the complete set of GIM runs. The coefficients of this orthonormal expansion are themselves represented by simple functions of solar activity, equatorial drift, and thermospheric winds.

The conversion from vertical TEC to slant TEC is accomplished by integrating model electron den-

sity along the line of sight rather than applying an obliquity factor to the vertical TEC. Although the obliquity factor works well at mid latitudes, it can be very inaccurate in the equatorial anomaly or anywhere there are large spatial gradients.

### 4. Model input parameters

The model requires the date and time (UT) and the location of the observer, the solar activity level, and the equatorial drift and thermospheric wind parameters for the longitude of the user. If drift and wind parameter values are not available, the model uses climatological estimates.

### 5. Publication references

**5.1** Daniell, R.E., L.D. Brown, and R.W. Simon (1996), "A New, Improved Ionospheric Correction Algorithm for Single Frequency GPS Receivers," *Proceedings of ION GPS-96*, Institute of Navigation, Alexandria, VA, pp. 635–640.

**5.2** Daniell, R.E., L.D. Brown, and R.W. Simon (1997), "Performance Comparisons Between the Current and a New Prototype Single Frequency Ionospheric Correction Algorithm," *Proceedings of the 53rd Annual Meeting*, Institute of Navigation, Alexandria, VA, pp. 101–106.

### 6. Dates of development, authors, and sponsors

**6.1 Dates:** 1996–1998.

**6.2 Authors:** R.E. Daniell, L.D. Brown, and R.W. Simon.

**6.3 Sponsors:** Computational Physics, Inc. (CPI) under a Small Business Innovation Research (SBIR) contract with the Air Force Research Laboratory.

### 7. Model codes and sources

Under the terms of the SBIR program, the model is a proprietary product of CPI, although the government retains certain rights to license the software. Others may contact CPI to obtain licensing information: Robert E. Daniell Jr., Computational Physics, Inc., Suite 202A, 240 Bear Hill Road, Waltham, MA 02154-1026, tel. 781/487-2250, FAX 781/487-2290 (e-mail daniell@cpiboston.com).



# **American Institute of Aeronautics and Astronautics**

**1801 Alexander Bell Drive, Suite 500  
Reston, VA 20191-4344**



**ISBN 1-56347-347-X**